



## Using mercury and lead stable isotopes to assess mercury, lead, and trace metal source contributions to Great Salt Lake, Utah, USA

Samuel F. Lopez <sup>a,b</sup>, Sarah E. Janssen <sup>c,\*</sup>, Michael T. Tate <sup>c</sup>, Diego P. Fernandez <sup>a</sup>, Christopher R. Anderson <sup>a</sup>, Grace J. Armstrong <sup>c</sup>, Thomas C. Wang <sup>c</sup>, William P. Johnson <sup>a,\*</sup>

<sup>a</sup> Department of Geology and Geophysics, University of Utah, Salt Lake City, UT 84112, United States

<sup>b</sup> U.S. Geological Survey, Utah Water Science Center, West Valley City, UT 84119, United States

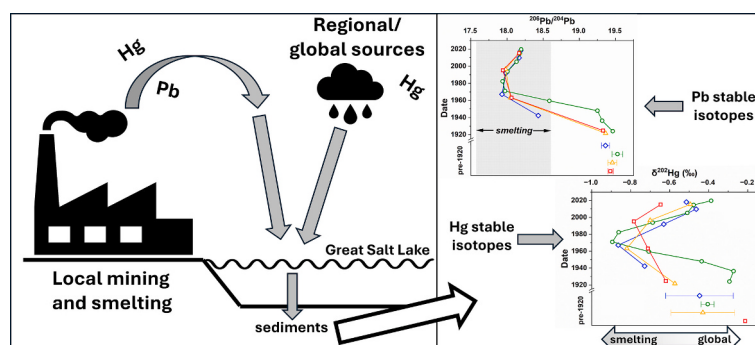
<sup>c</sup> U.S. Geological Survey, Upper Midwest Water Science Center, Madison, WI 53726, United States



### HIGHLIGHTS

- Metal sources in Great Salt Lake sediments were assessed with Hg/Pb isotopes.
- Pb isotope values in post-1920 sediments indicate local mining/smelting sources.
- Pre-1920/post-2000 Hg inputs are mainly atmospheric and of regional/global origin.
- Hg inputs during the 20th century were dominated by local mining/smelting sources.
- Other metals show correspondence with Hg/Pb, indicating mining/smelting influence.

### GRAPHICAL ABSTRACT



### ARTICLE INFO

Editor: Xinbin Feng

#### Keywords:

Great Salt Lake  
Mercury  
Lead  
Metals  
Stable isotopes  
Mining  
Smelting  
Pollution

### ABSTRACT

Great Salt Lake is a critical habitat for migratory birds that is threatened by elevated metal concentrations, including mercury (Hg) and lead (Pb), and is subject to severe hydrologic changes, such as declining lake level. When assessing metal profiles recorded in Great Salt Lake sediment, a large data gap exists regarding the sources of metals within the system, which is complicated by various source inputs to the lake and complex biogeochemistry. Here, we leverage Hg and Pb stable isotopes to track relative changes in metal source contributions to Great Salt Lake over time. Mercury and Pb concentrations increase in sediments deposited after 1920 and peak between 1965 and 1995, following closure of several local smelters and the onset of increased emission controls. The nominal associations above are confirmed via Hg stable isotopes in pre-1920 background sediments, which reflect atmospheric inputs from regional and global origin, whereas Hg and Pb stable isotopes together indicate that elevated metal concentrations in mid-late 20th century sediments reflect increased mining/smelting inputs. The observed minimal rebound towards pre-1920 Pb isotope signatures in 21st century sediments indicates that mining/smelting inputs, though reduced, remain a primary source of Pb to Great Salt Lake. In contrast, the more pronounced rebound of Hg stable isotope signatures to pre-1920 values indicate a greater contribution of atmospheric inputs of regional/global origin to current Hg inputs, though Hg concentrations are ~10 times greater than pre-1920 background values due to global increases in atmospheric Hg concentrations or possibly slow

\* Corresponding authors.

E-mail addresses: [sjanssen@usgs.gov](mailto:sjanssen@usgs.gov) (S.E. Janssen), [william.johnson@utah.edu](mailto:wiliam.johnson@utah.edu) (W.P. Johnson).

recovery from local contamination. The importance of regional/global Hg sources to the system suggests that reductions in Hg bioaccumulation in the open water food webs of Great Salt Lake are more dependent on national and global reductions in Hg emissions and management strategies to limit methylmercury production within system. This work highlights the utility of using coupled Hg and Pb stable isotope values to assess trace metal pollution sources and pathways in aquatic systems.

## 1. Introduction

Great Salt Lake, a large terminal lake adjacent to the rapidly growing Wasatch Front metropolitan area of over 2.6 million people, is a vital habitat for millions of birds and is recognized as a “Site of Hemispheric Importance” by the Western Hemisphere Shorebird Reserve Network (Aldrich and Paul, 2002). Though the high salinity of the open waters prohibits the survival of fish and most invertebrate species, Great Salt Lake supports robust populations of brine shrimp (*Artemia*) and brine flies (*Ephydriidae*) which are an important food source to pelagic-feeding birds, including the Eared Grebe (*Podiceps nigricollis*), Wilson’s Phalarope (*Phalaropus tricolor*), Common Goldeneye (*Bucephala clangula*), Northern Shoveler (*Spatula clypeata*), and California Gull (*Larus californicus*; Conover and Bell, 2020). Over 10 million shorebirds and waterfowl utilize Great Salt Lake and its surrounding wetlands for breeding activities and/or during portions of biannual migrations (Aldrich and Paul, 2002; Great Salt Lake Ecosystem Program, 2023). Large fractions of several species’ global populations utilize Great Salt Lake in this manner, including 50 % of Eared Grebes and ~30 % of Wilson’s Phalaropes during staging (Conover and Bell, 2020).

In 2007, waterfowl consumption advisories were implemented for three species of duck from Great Salt Lake: Northern Shoveler, Common Goldeneye, and Cinnamon Teal (*Spatula cyanoptera*), which were found to have elevated mercury (Hg) levels exceeding the Environmental Protection Agency (EPA) screening value of 0.3 µg/kg (wet weight) in breast muscle tissue (Scholl and Ball, 2005, 2006). These advisories, unique in the United States for avian species, raised public concern regarding wildlife and human health and prompted additional investigation that discovered the anoxic, sulfidic, and organic-rich bottom waters of Great Salt Lake are distinguished by high concentrations of methylmercury (MeHg), the more neurotoxic and bioaccumulative form of Hg (Driscoll et al., 2013), that can exceed 30 ng/L (Naftz et al., 2008; Valdes et al., 2017; Yang et al., 2019). Methylmercury concentrations can also exceed 5 ng/L in the shallow surface waters of Great Salt Lake (Peterson and Gustin, 2008), and 10 ng/L in shallow porewaters of adjacent wetlands (Johnson et al., 2015). These MeHg concentrations are much higher than concentrations measured in other locations throughout the United States. In a recent survey of 87 lentic, lotic, and wetland waterbodies throughout the United States, the maximum MeHg value observed was 2.1 ng/L (Nelson et al., 2024). Additionally, other trace elements are elevated in the water column and sediments of Great Salt Lake, though selenium (Se), which is another contaminant of particular concern due to risk to migratory birds, is the only trace element subject to a Great Salt Lake-specific water quality standard (Ohlendorf et al., 2009).

Mercury enters Great Salt Lake through direct atmospheric deposition (wet and dry) following short- or long-range transport, through watershed inputs (including the Bear, Jordan, and Weber Rivers), and through direct industrial discharge (Naftz et al., 2009). Because Great Salt Lake is a terminal lake with no tributary outflows, pathways for Hg removal from the water column include photoreduction and evasion in the upper water column, uptake by biota and subsequent transport away from the lake (e.g., brine shrimp harvest), and deposition to sediments. Sedimentation is an important pathway for Hg and trace element removal from the water column, and the historical record of trace element deposition in Great Salt Lake is therefore recorded in its accumulated sediments (Naftz et al., 2009; Oliver et al., 2009; Wurtsbaugh et al., 2020). However, relatively few studies have examined sources of

Hg and other trace metals to Great Salt Lake (Diaz et al., 2009; Naftz et al., 2009; Wurtsbaugh et al., 2020), and none have utilized isotopic tracers to establish direct connections to sources.

Stable isotope tracers can reveal relationships to sources as well as in-lake processes that impact contaminant fate and transport. Changes to the distribution of metal stable isotopes (Hg and lead [Pb]) are driven by fractionation during kinetic and equilibrium reactions, termed mass dependent fractionation (MDF) (represented by  $\delta^{202}\text{Hg}$  for Hg). In certain isotope systems, such as Hg, mass independent fractionation (MIF) can also occur during photochemical exposure (Bergquist and Blum, 2007), allowing for examination of photochemical reduction in the water column (tracked by  $\Delta^{199}\text{Hg}$  and  $\Delta^{201}\text{Hg}$ ), or photochemical oxidation of Hg in the upper atmosphere (tracked by  $\Delta^{200}\text{Hg}$  and  $\Delta^{204}\text{Hg}$ ) (Tsui et al., 2020), the latter of which provides a conservative tracer for Hg in atmospheric deposition from regional and global sources. Differences in the extent of fractionation can record distinct mercury sources (e.g., industrial effluent vs atmospheric deposition) and provide insight into processes such as atmospheric transport and photochemical degradation. For example, Hg stable isotopes have been used to apportion atmospheric deposition, terrestrial runoff, and industrial sources of Hg in sediments (Janssen et al., 2021; Lepak et al., 2015), and have been used to trace Hg contamination from smelting emissions (Ma et al., 2013). Likewise, Pb stable isotope ratios, which are not significantly altered during industrial processes such as smelting, have also been used to distinguish between mining and background sources of Pb in lake sediments (Ettler et al., 2006; Monna et al., 2000; Reynolds et al., 2009; Shiel et al., 2010), and to fingerprint contributions from coal combustion and the use of leaded-gasoline (Chow and Earl, 1972; Teutsch et al., 2001).

Based on previous assessments of Great Salt Lake, atmospheric deposition and non-ferrous metal production (mining and smelting) are recognized as important sources of Hg and trace elements (Naftz et al., 2009; Peterson and Gustin, 2008; Wurtsbaugh et al., 2020), but it remains unclear how the relative source contributions of Hg and other trace element sources have changed through time. Additionally, understanding the current relative source contributions would be useful for management of Great Salt Lake bird habitat, particularly if there is potential to limit current metal inputs from local sources. This study utilizes Hg and Pb stable isotope measurements on four dated Great Salt Lake sediment cores to directly assess historical and current contributions of atmospheric, terrestrial runoff, and industrial sources to Hg and other trace metals in Great Salt Lake sediments. Examining the sources and distribution of metals in Great Salt Lake sediments is also relevant given that the impact to adjacent metropolitan and suburban air quality originating from exposure of lakebed sediment in response to a shrinking Great Salt Lake has received national press (Flavelle, 2022; Tempest Williams, 2023) and scientific attention (Perry et al., 2019; Putman et al., 2023).

## 2. Materials and methods

### 2.1. Study area

Utah is the third largest metal-producing state in the United States (Utah Geological Survey, 2024), with several of its largest mining districts (Bingham Canyon, Tintic, Mercur, and Park City districts) falling within the Great Salt Lake watershed (Fig. S1). This includes the world’s largest open pit mine (Bingham Canyon Mine) (Utah Geological Survey,

2024), located near the south shore of Great Salt Lake, along with its associated smelter (Garfield Smelter) and tailings pile, both located directly on the south shore. Historically, Bingham Canyon is the most productive mining district in the United States, and has produced copper, molybdenum, gold, silver, lead, and zinc (Utah Geological Survey, 2024). The Bingham Canyon Mine opened in 1905, while other smaller mining operations, particularly in the Park City district of the Wasatch Range, began during the second half of the 18th century (Wurtsbaugh et al., 2020). In addition to mining activity, several associated smelters were present throughout the Salt Lake Valley (Fig. S1), with the first smelting operations beginning the late 19th century (U.S. EPA, 2024). Most smelters in the area ceased operation in the 1960s and 1970s following the Clean Air Act; however, the Garfield Smelter, which is within 2 km of the southern shoreline of Great Salt Lake, is still in operation. A taller 370 m stack was constructed in the mid-1970s with better emission controls and is likely better at dispersing emissions away from the lake (Reynolds et al., 2009; Wurtsbaugh et al., 2020). Detailed summaries of metals production and mining/smelting activities in the vicinity of Great Salt Lake can be found elsewhere (Wurtsbaugh et al., 2020).

## 2.2. Sediment core collection and processing

Four sites along a north-south transect were established in Gilbert

Bay for sediment core collection (CB2, N1018, 3510, and GB14) (Fig. 1). Coring was not attempted in Gunnison Bay due to the presence of a largely impenetrable salt layer on the lake bottom. Deeper sites (ranging from approximately four to seven meters at the time of sampling) were targeted for sample collection, because this limited disruptions to the sediment record from bioturbation from foraging waterfowl and sediment resuspension due to wind/wave generation. Sediment cores were collected in 2021 via gravity corer equipped with acid washed acrylic tubing. Care was taken to preserve the sediment-water interface during sampling and transport from the field to the laboratory. In the laboratory, cores were sectioned in 2 cm increments within 12 h of collection and stored frozen at -20 °C in high density polyethylene (HDPE) jars. Core sections were freeze dried until constant mass was achieved, and weights were recorded before and after freeze drying to calculate water content. Dry sediments were homogenized via mortar and pestle or ball mill and stored in borosilicate vials until analysis.

Due to the high salt content of Great Salt Lake porewaters, salt content of dried sediment varies with porosity, and can exceed 40 % in unconsolidated sediments (Oliver et al., 2009; Wurtsbaugh et al., 2020). Accounting for salt content was necessary to calculate sediment bulk density values, which were used in Pb-210 dating, and to correct trace element concentrations. Approximately 1 g of dry sediment was placed in a tared volumetric flask, weighed, and filled to the mark with ultra-high purity water. The water/sediment solution was mixed and left to

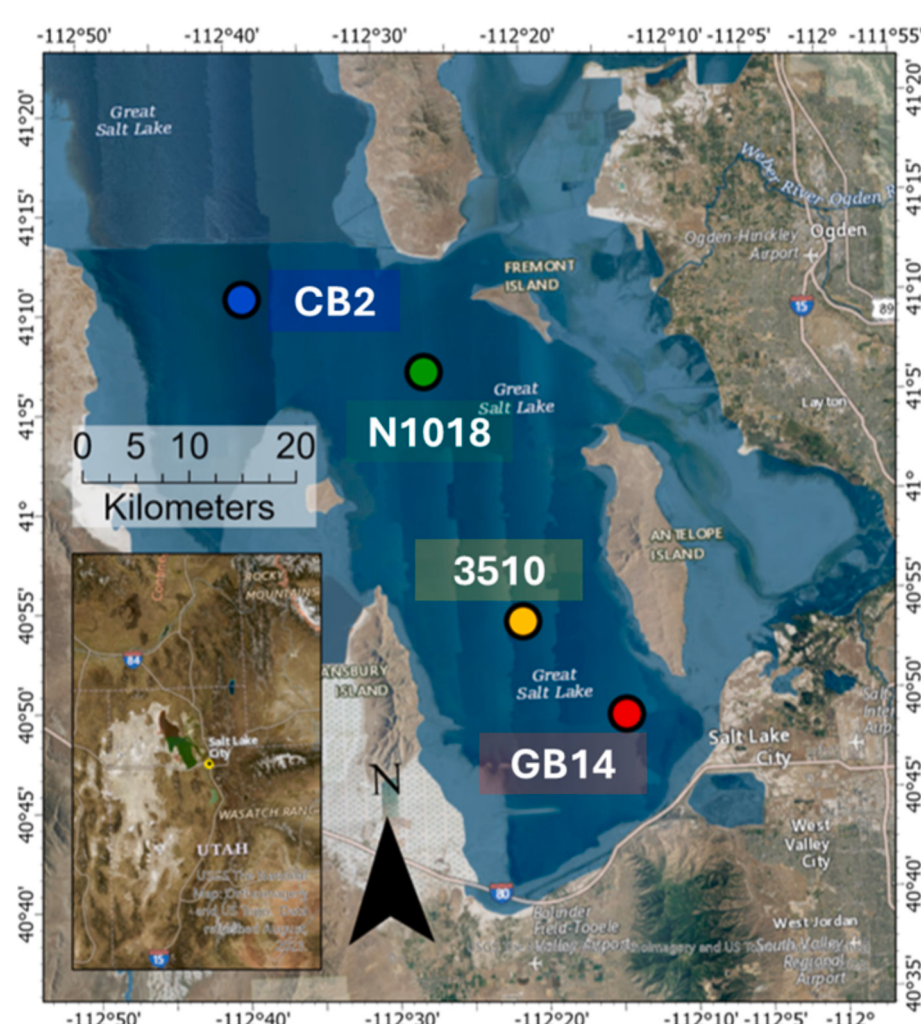


Fig. 1. Sites of sediment core collection at Great Salt Lake, Utah.

sit for 24 h. After 24 h, additional water was added to the mark as needed. The density of the solution in the volumetric flask for each sediment core section was then measured at 20 °C using an Anton Paar DMA 35n portable density meter (Anton Paar USA Inc., Ashland, VA). The difference between the density of ultra-high purity water and the density of the solution was attributed to the weight of dissolved salt, which was used to calculate the salt content of the dry sediment sample originally added to the flask.

### 2.3. Watershed sampling

To constrain potential Hg contributions from terrestrial runoff to Great Salt Lake sediments, surficial sediment grab samples ( $n = 2$ ) were collected at each of seven tributary sites: Bear River, Weber River, Jordan River, Lee Creek, Silver Creek, Little Cottonwood Creek, and the Kennecott Tailings Outfall. These samples were collected during spring/summer of 2023 during high-water conditions following a robust 2022/2023 winter snowpack (Fig. S1). General high-water conditions were targeted, because we assumed that samples represent periods where watershed Hg fluxes to Great Salt Lake are highest. Depositional zones were explicitly targeted to obtain samples representative of sediments most likely to be mobilized downstream to Great Salt Lake. Due to safety logistics arising from high-water conditions, two sites (Surplus Canal and Weber River) were sampled on later dates than the other five sites.

Tributary sampling locations were classified as mining impacted, urban impacted, and/or unimpacted according to their proximity to mining/smelting operations and according to land coverage within the Bear, Weber, and Jordan River watersheds. More information about land use and mining classification for tributary sampling locations can be found in the Supporting Information.

### 2.4. Precipitation collection

Rainfall samples were collected at two sites in West Valley City, UT and Bountiful, UT, two cities near the southern and southeastern shores of Great Salt Lake, respectively. An acid-washed bucket was deployed immediately prior to rainfall events. The bucket was equipped with a large acid-washed funnel to limit evaporation. Rainfall samples were transferred to 500 mL polyethylene terephthalate glycol (PETG) bottles no later than 1 h after the end of rainfall events, acidified to 1.0% trace metal grade hydrochloric acid (HCl), and were stored in a cool dark environment until further processing and analysis.

### 2.5. Age dating by Pb-210

The four sediment cores were dated using  $^{210}\text{Pb}$  at the St. Croix Watershed Research Station (Marine on St. Croix, Minnesota).  $^{210}\text{Pb}$  chronologies were determined using the constant-flux constant sedimentation (CF:CS) model (Appleby and Oldfield, 1992), and a single dry mass sediment accumulation rate (DMAR) was estimated for each core. Estimating a single DMAR for each core was sufficient to address the primary goal of this study, which was to utilize stable isotope tracers to assess large scale changes in trace metal source contributions over the past ~100 years. Higher resolution trace metal chronologies in Great Salt Lake sediment cores are reported elsewhere (Wurtsbaugh et al., 2020). Salt-free dry bulk densities (estimated from water and salt content) were used in determination of chronologies and DMARs to correct for the influence of salinity. Due to a combination of relatively low total  $^{210}\text{Pb}$  activity in all four cores relative to background supported values (3–4 pCi/g in surficial sediments vs ~1.3 pCi/g at depth) (Fig. S2), relatively coarse sectioning resolution (2 cm), and low sedimentation rates, reliable chronologies could only be determined for the past ~70–100 years. However, chronologies were of sufficient length to encompass changes in Hg, Pb, and other trace metal deposition from 1925 to 1955 through present day, the target period of this study.

### 2.6. Hg analysis

Mercury analysis of sediment and water (rainfall) samples was performed at the U.S. Geological Survey Mercury Research Laboratory (USGS MRL, Madison, WI). Approximately 0.5 g of each sediment sample was digested in 3:1 v/v HCl: nitric acid ( $\text{HNO}_3$ ), termed aqua regia, on a heating block set to 75 °C for 5 h. Because Great Salt Lake sediments are carbonate rich, digests were left overnight at room temperature after initial acid addition to prevent excess foaming during heating. Digests were diluted to 50 % acid with ultra-high purity water immediately following heating. Acidified water samples for total Hg concentration analysis were pre-treated with ultraviolet (UV) light for 2–3 days to degrade organic carbon interferences prior to total Hg analysis. Immediately after UV treatment, samples were oxidized using bromine monochloride to a final concentration of 1% (v/v) and heated at 55 °C for five days. Sediment digests and waters were analyzed according to a modified version of U.S. EPA Method 1631 (U.S. EPA, 2002). Certified reference materials (CRMs), International Atomic Energy Agency (IAEA) 456 (Natural Marine Sediment,  $n = 11$ ) and National Institute of Standards and Technology (NIST) 1944 (New York/New Jersey Harbor Sediment,  $n = 6$ ) were digested with each batch of sediments, and recoveries were  $95 \pm 10\%$  (average  $\pm$  standard deviation [SD]) of certified values. All quality control and quality assurance data for Hg concentration measurements are provided in the associated U.S. Geological Survey data release (doi:<https://doi.org/10.5066/P13XSQWN>) (Lopez et al., 2024).

### 2.7. Hg stable isotope analysis

Sediment digestions analyzed for Hg were diluted to <10 % acid content and analyzed for Hg stable isotopes using a multicollector inductively coupled mass spectrometer (MC-ICP-MS) at the USGS MRL. Briefly, sediments were analyzed using standard-sample bracketing with NIST 3133 (inorganic Hg standard) (Blum and Bergquist, 2007). Dilutions of bracketing standards and secondary standards (NIST RM 8610, "UM Almaden") were matrix (e.g., <10 % aqua regia) and Hg concentration (0.5 – ng mL<sup>-1</sup>) matched to samples prior to analysis. Samples and standards were introduced to the MC-ICP-MS via tin (II) chloride reduction within a custom gas liquid separator (Yin et al., 2016). A thallium standard (40 ng mL<sup>-1</sup>) was simultaneously introduced for mass bias correction. Tuning parameters on the MC-ICP-MS were optimized to produce a > 1 V response for a 1 ng mL<sup>-1</sup> Hg solution and are outlined elsewhere (Janssen et al., 2019; Yin et al., 2016). Measurement accuracy and precision were assessed using the NIST RM 8610 secondary standard (one for every five samples) and the CRM NIST 1944 (Table S1) and were consistent with previously published assessments (Blum and Johnson, 2017). Literature data are not available on the Hg isotopic composition of IAEA 456, but replicate digests demonstrated similar external precision (2 SD:  $\delta^{202}\text{Hg} = 0.13\%$ ,  $\Delta^{199}\text{Hg} = 0.09\%$ ,  $\Delta^{200}\text{Hg} = 0.04\%$ ,  $n = 10$ ) to other CRMs. Isotopic data on all CRMs and standards are provided in the associated U.S. Geological Survey data release (Lopez et al., 2024) and in Table S1 of the Supporting Information.

Mercury isotope results are expressed in delta notation in reference to NIST 3133 and were calculated according to convention (Blum and Bergquist, 2007). MDF is expressed by a lowercase delta ( $\delta$ ) and calculated by Eq. (1):

$$\delta^{\text{xxxHg}} (\%) = \left[ \left( \frac{\text{xxxHg}}{^{198}\text{Hg}} \right)_{\text{sample}} / \left( \frac{\text{xxxHg}}{^{198}\text{Hg}} \right)_{\text{NIST-3133}} - 1 \right] \times 1000 \quad (1)$$

MIF data is signified by an uppercase delta ( $\Delta$ ) and can be calculated by Eq. (2):

$$\Delta^{\text{xxxHg}} (\%) = \delta^{\text{xxxHg}} - (\delta^{202}\text{Hg}^* \beta) \quad (2)$$

where  $\beta$  represents the mass scaling factor, an isotope-specific constant determined by the theoretical laws of MDF (Blum and Bergquist, 2007).

### 2.8. Other trace element analysis

All trace metal analyses were conducted in a filtered air positive pressure lab at the University of Utah, and all samples, digests, and dilutions were handled under laminar flow benches. Approximately 50 mg of each freeze-dried and homogenized sediment sample was transferred into a 7 mL Polytetrafluoroethylene (PTFE) digestion vial, with 2 mL of trace metal grade (TMG) hydrofluoric acid (HF) and 1 mL TMG HNO<sub>3</sub>. The vial was then closed using two round-shaped pliers and placed in a hot plate inside a PTFE-coated block at 165 °C for three days. About 10 % of vials lost a small fraction of the total volume, and rare cases of substantial volume reduction (>50 %) required the addition of more acids. Following digestion, the liquid was evaporated from the sample at 150 °C, followed by addition of 2 mL concentrated HCl. The vial was closed with pliers and placed in a hot plate inside a block at 165 °C for two days with occasional manual stirring. Digests were diluted with 3 mL of ultra-high purity water following heating. Using the masses of dry sediment and final digest, the solution factor was calculated for each sediment, with values around 80. These digests were then diluted volumetrically by a factor of 100 with 2.4 % HNO<sub>3</sub>, and subsequently analyzed for 43 elements using an external calibration curve with internal standard.

Elemental quantification was performed with a triple quadrupole inductively coupled plasma mass spectrometer (ICP-MS, Agilent 8900, Santa Clara, California). An external calibration curve was prepared from 1000 mg/L single element standards (Inorganic Ventures, Christiansburg, VA). An indium (IN, 10 ng mL<sup>-1</sup>) internal standard was added to all samples, calibration solutions, and blanks that were then introduced to the ICP-MS using a dual-pass quartz spray chamber, PTFE nebulizer, dual-syringe introduction system (Teledyne, AVX 71000), platinum cones, and sapphire injector in a platinum-shielded quartz torch. The limits of determination (LoD) were calculated as three times the standard deviation of the blanks, multiplied by the total dilution factor used for samples. Average recoveries for Pb on three USGS reference materials were consistent with certified values (CRD-1: 125 ± 4 %, n = 4; AGV-1: 104 ± 4 %, n = 4; SBC-1: 105 ± 4 %, n = 4). Certified concentration values and recoveries for all trace elements obtained with the methodology used are provided for the three CRMs in Table S2, and all data from measurements on samples and CRMs can be found in the associated U.S. Geological Survey data release (Lopez et al., 2024).

### 2.9. Pb stable isotope analysis

Aliquots from trace element digests containing 50 ng of Pb were mixed with concentrated HNO<sub>3</sub> and water to 6 M HNO<sub>3</sub> to a volume of 0.5 mL and purified using a 50 mL chromatographic column containing Sr-spec resin (100–150 mm, Eichrom Technologies, Lisle, IL). After matrix rinse with 6 column volumes (CV) of 6 M HNO<sub>3</sub>, Sr was eliminated with 6 CV of water, and the Pb fraction was eluted with 16 CV of 0.1 M citric acid at pH = 5 with recoveries >98 %. Lead fractions were acidified to 5 % HNO<sub>3</sub> and spiked with 25 ng mL<sup>-1</sup> Tl (Thallium Metal, NIST 997). Lead fractions were run for Pb isotopic ratios via MC-ICP-MS (Neptune, Thermo Scientific, Bremen, Germany) with a quartz double-pass spray chamber and platinum cones. Reported Pb isotope values herein are expressed as ratios with <sup>204</sup>Pb in the denominator (<sup>206</sup>Pb/<sup>204</sup>Pb, <sup>207</sup>Pb/<sup>204</sup>Pb, <sup>208</sup>Pb/<sup>204</sup>Pb). For mass bias correction, <sup>203</sup>Tl/<sup>205</sup>Tl = 0.418913 was used. Reference material NIST 981 (Lead Metal) was used to verify the quality of data. NIST 981 aliquots in 6 M HNO<sub>3</sub>, or “column standards”, were purified and run as samples. In addition, a 50 ng mL<sup>-1</sup> Pb solution of NIST 981 in 5 % HNO<sub>3</sub> and containing 25 ng mL<sup>-1</sup> Tl was run repeatedly with samples in the MC-ICP-MS (1 standard every 3 samples). Table S3 displays the long-term Pb isotopic average ratios obtained for NIST 981 (no column), compared

with the average values run through purification columns during the same sessions when samples were purified.

### 2.10. Data analysis

All data visualization and analyses were performed in OriginPro 2023 (OriginLab Corporation, Northampton, MA). Relationships between constituent concentrations and Hg and Pb isotope values were evaluated using Spearman correlation tests at the  $p < 0.05$  and  $p < 0.01$  levels. To assess source contributions, Hg and Pb isotope values in Great Salt Lake sediment cores were qualitatively compared to reference values derived from literature, termed “endmembers.” Briefly, Pb isotope values in Great Salt Lake sediment cores were qualitatively compared to ranges in northern Utah ores that were likely to have been mined and smelted in the vicinity of Salt Lake Valley (Reynolds et al., 2009; Stacey et al., 1968), as well as values in Rocky Mountain region coals (Chow and Earl, 1972) and U.S. leaded gasoline (Teutsch et al., 2001). Hg isotopes values in Great Salt Lake sediment cores were qualitatively compared to those in Rocky Mountain region precipitation samples (Kurz et al., 2019), as well as in total gaseous mercury (TGM) samples previously collected adjacent to Great Salt Lake (Tate et al., 2023). A Hg isotope endmember specific to mining and smelting was estimated based on Hg isotope signatures in Great Salt Lake sediment core sections that correspond to peak Pb concentrations. Greater discussion of endmember derivation can be found in the Results and Discussion.

## 3. Results and discussion

### 3.1. Sediment chronologies

Sedimentation rates, revealed by age-depth relationships (slope in Fig. 2), are lowest (and practically equivalent) for cores GB14 and 3510 (0.036 g/cm<sup>2</sup>/yr and 0.035 g/cm<sup>2</sup>/yr, respectively), intermediate for core CB2 (0.055 g/cm<sup>2</sup>/yr), and highest for core N1018 (0.110 g/cm<sup>2</sup>/yr) (Fig. 2), which are in close agreement with sedimentation rates (0.02 to 0.13 g/cm<sup>2</sup>/yr) previously documented at overlapping sites and similar areas of Great Salt Lake (Oliver et al., 2009). The higher sedimentation rates observed at site N1018 are likely due to its location south of a bathymetric high (sill) that bisects the south arm (Baskin, 2005; Jewell, 2021), over which north-to-south bottom-water currents flow (Beisner et al., 2009; Jewell, 2021), creating conditions favorable for higher leeward sedimentation rates (Oliver et al., 2009). Despite relatively high sedimentation rates at site CB2, reliable chronologies could not be determined for sediments deposited prior to the mid-1950s. It is possible that the construction of the railroad causeway in the late

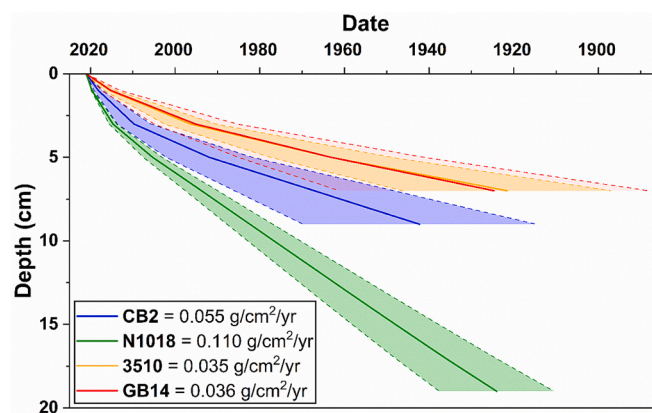


Fig. 2. Age-depth profiles and sedimentation rates for four Great Salt Lake sediment cores. Solid lines represent age-depth relationships, while dashed lines and shaded regions represent age uncertainties of CF:CS models.

1950s five km north of site CB2 initiated increased sedimentation by altering lake currents (Oliver et al., 2009). However, chronologies were of sufficient length in all four cores to encompass 1925–1955 through present day, the target period of this study. We assume that sediments associated with depths lacking measurable unsupported  $^{210}\text{Pb}$  were deposited prior to 1920.

### 3.2. Trace metal and isotope composition of Great Salt Lake sediment cores

Mercury (Fig. 3a), Pb (Fig. 3b), and other trace element (Fig. 4) concentrations in Great Salt Lake sediment cores show peak concentrations corresponding to a three-decade period (approximately 1965–1995), overlapping with the period of heaviest industrial activity prior to reduction in mining and smelting activities and improved pollution control technologies which yielded decreasing loads to the system (Wurtsbaugh et al., 2020). The timing of peak Hg concentrations was earlier in the core collected at CB2 (1967), while differences in peak Hg concentration timing in the other three cores (1993–1996) were within dating uncertainty. The differences in peak timing between the CB2 core and other three cores may be related to differences in site location; CB2 sits within Carrington Bay, the northwest portion of Gilbert Bay, which is separated by a bathymetric sill from the other coring sites in the southeast portion of Gilbert Bay (Fig. 1). Regardless, peak timing (1965–1995) in the four cores collected from locations

spanning the south arm of Great Salt Lake generally corroborates those from two previous sediment cores collected from the southern portion of the south arm (Wurtsbaugh et al., 2020). The source of Pb, Hg, and other trace elements was previously concluded to be mining and smelting based on indirect evidence such as correspondence of peak concentrations to Utah metals production and the onset of industrial emissions controls (Wurtsbaugh et al., 2020).

Lead stable isotope measurements (Fig. 3d) show a shift from background (pre-1920)  $^{206}\text{Pb}/^{204}\text{Pb}$  ratios (19.5) to a minimum (17.9) coinciding with peak Pb concentrations (1965–1995), with a subsequent partial rebound to present day ratios (18.2). The minimum and present-day  $^{206}\text{Pb}/^{204}\text{Pb}$  ratios (17.6–18.6) (Fig. 3d) correspond with those of northern Utah ores smelted increasingly throughout the 20th century (Reynolds et al., 2009; Stacey et al., 1968). Lead stable isotope chronologies are consistent with those of cores collected from alpine lakes in the Uinta Mountains east of Great Salt Lake shown to be impacted by smelting operations in Salt Lake Valley (Reynolds et al., 2009).

Contributions of other sources to elevated sediment Pb concentrations, specifically coal combustion and leaded gasoline, were also considered. However,  $^{208}\text{Pb}/^{206}\text{Pb}$  and  $^{206}\text{Pb}/^{207}\text{Pb}$  ratios (Fig. S3) in Great Salt Lake sediments with elevated Pb are dissimilar to the composition of coal samples collected from the Rocky Mountain province of North America (Chow and Earl, 1972) (Fig. S4). Additionally,  $^{208}\text{Pb}/^{206}\text{Pb}$  and  $^{206}\text{Pb}/^{207}\text{Pb}$  ratios in these sediments are generally distinct from Pb ratios in U.S. leaded gasoline (Teutsch et al., 2001) (Fig.

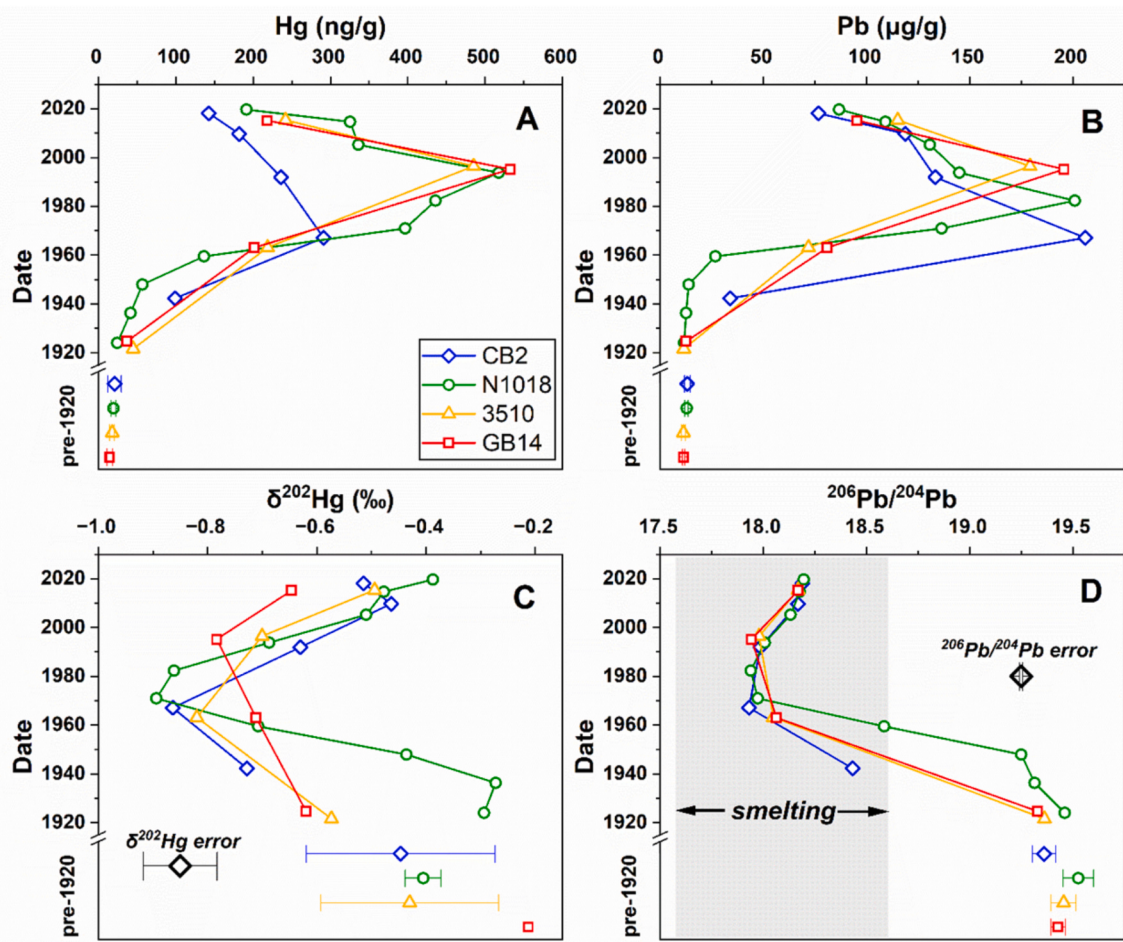


**Fig. 3.** a) Hg and b) Pb concentrations, and c)  $\delta^{202}\text{Hg}$ , and d)  $^{206}\text{Pb}/^{204}\text{Pb}$  measurements in four dated Great Salt Lake sediment cores. Generic error bars represent the 2 SD of measurements on IAEA 456 ( $n = 6$  for  $\delta^{202}\text{Hg}$ ) and 2 SD of measurements on AGV-1 ( $n = 4$ ) for  $^{206}\text{Pb}/^{204}\text{Pb}$ . The shaded region represents the known Pb isotope composition of galena-bearing ores mined and smelted proximal to Great Salt Lake ( $^{206}\text{Pb}/^{204}\text{Pb} = 17.6\text{--}18.6$ ) (Reynolds et al., 2009; Stacey et al., 1968). Error bars on pre-1920's background values represent the 1 SD of sample values associated with depths lacking measurable unsupported  $^{210}\text{Pb}$  (CB2:  $n = 8$ ; N1018:  $n = 5$ ; 3510:  $n = 5$ ; GB14:  $n = 7$ ).

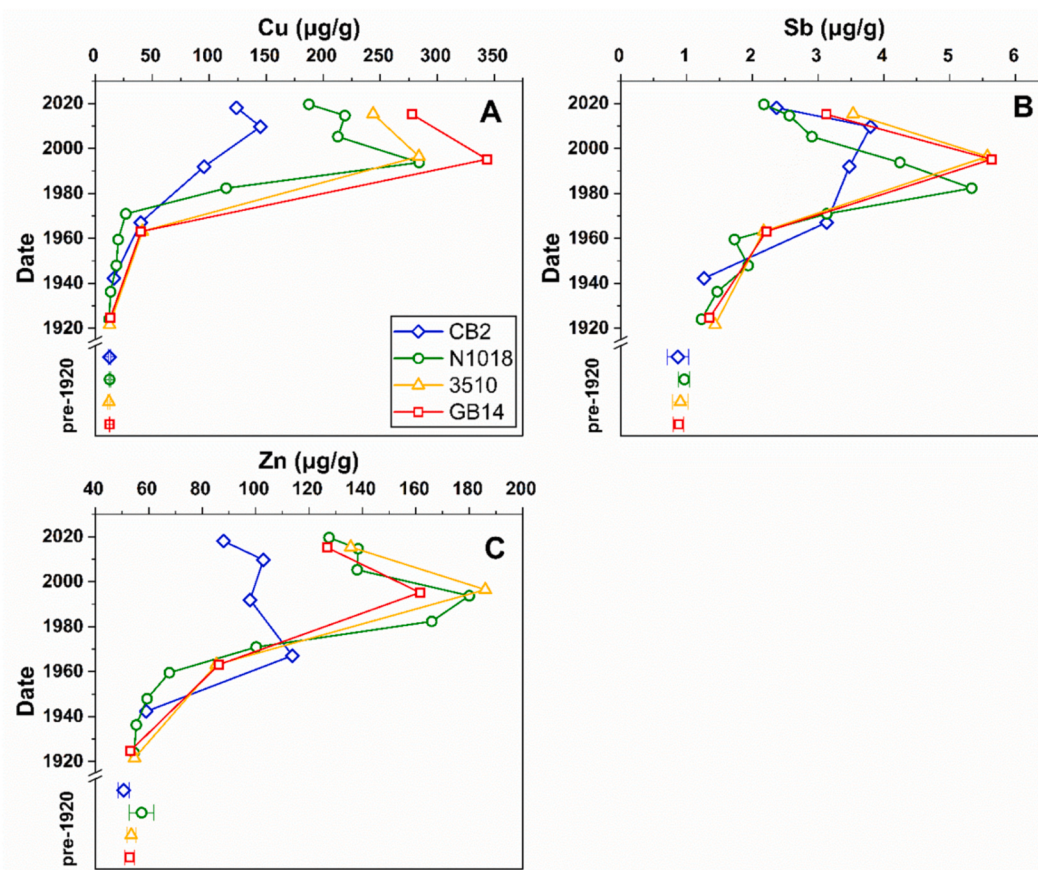


**Fig. 4.** a) Cu, b) Sb, and c) Zn measurements in four dated Great Salt Lake sediment cores. Error bars on pre-1920's background values represent the 1 SD of sample values associated with depths lacking measurable unsupported  $^{210}\text{Pb}$  (CB2: n = 8; N1018: n = 5; 3510: n = 5; GB14: n = 7).

S4). In cores collected from Uinta Mountain lakes in 2001, increases in  $^{206}\text{Pb}/^{207}\text{Pb}$  (to 1.18) and  $^{206}\text{Pb}/^{204}\text{Pb}$  (to 18.4) were attributed to minor contributions (20–30 %) of gasoline-derived Pb from 1960 to 1980 mixing with smelting-derived Pb (70–80 %) (Reynolds et al., 2009). However, the more recently collected Great Salt Lake sediment cores exhibit a slow rebound towards present day that does not appear to be caused by the use of leaded gasoline throughout the 20th century, and most recently deposited sediments display lower  $^{206}\text{Pb}/^{207}\text{Pb}$  (~1.16) and  $^{206}\text{Pb}/^{204}\text{Pb}$  (~18.2) signatures than those observed in Uinta Mountain lake sediments, which were influenced by minor (20–30 %) gasoline contributions (Reynolds et al., 2009). The less discernable influence of gasoline in Pb isotope chronologies in Great Salt Lake cores relative to those in Uinta Mountain lakes could be due to the closer proximity of Great Salt Lake coring sites to mining/smelting activity, or coarser sectioning resolution that obscures fine scale temporal trends (e.g., <10 years) in Pb isotope signatures. Regardless, Pb isotope signatures indicate local mining/smelting sources are more prominent in Great Salt Lake sediments with elevated Pb concentrations over contributions from unleaded gasoline and coal combustion.

In all four sediment cores, Hg stable isotope measurements show a shift from background  $\delta^{202}\text{Hg}$  values (Fig. 3c) ( $-0.41 \pm 0.15\text{‰}$ , n = 12) to lower values ( $-0.76 \pm 0.08\text{‰}$ , n = 4) coinciding with peak Hg concentrations (Fig. 3a), as well as peak Pb concentrations (Fig. 3b) and minima in  $^{206}\text{Pb}/^{204}\text{Pb}$  ratios (Fig. 3d), with subsequent rebound to present day values ( $-0.51 \pm 0.10\text{‰}$ , n = 4) (Fig. 3c). A combination of positive  $\Delta^{200}\text{Hg}$  and negative  $\Delta^{204}\text{Hg}$  is observed in both pre-1920 ( $\Delta^{200}\text{Hg}: 0.10 \pm 0.02\text{‰}$ ;  $\Delta^{204}\text{Hg}: -0.25 \pm 0.07\text{‰}$ , n = 12) and present-day ( $\Delta^{200}\text{Hg}: 0.7 \pm 0.02\text{‰}$ ;  $\Delta^{204}\text{Hg}: -0.10 \pm 0.02\text{‰}$ , n = 4) sediments (Fig. 5a and b), which is characteristic of wet atmospheric deposition (Chen et al., 2012; Demers et al., 2013; Kurz et al., 2019; Tsui

et al., 2020). Because  $\Delta^{200}\text{Hg}$  and  $\Delta^{204}\text{Hg}$  are thought to be conservative tracers of atmospheric processes (Chen et al., 2012), we conclude Hg isotope values of top Great Salt Lake sediment layers reflect atmospheric inputs and supports the conclusion of previous studies (Naftz et al., 2009; Peterson and Gustin, 2008) that atmospheric deposition dominates current Hg source contributions. At depths corresponding to peak Hg concentrations,  $\delta^{202}\text{Hg}$  ( $-0.76 \pm 0.08\text{‰}$ , n = 4),  $\Delta^{200}\text{Hg}$  ( $0.03 \pm 0.02\text{‰}$ , n = 4), and  $\Delta^{204}\text{Hg}$  ( $-0.05 \pm 0.02\text{‰}$ , n = 4) values are all significantly different (t-test,  $p < 0.05$ ) from both pre-1920 and present-day values. The fact that Hg stable isotope signatures corresponding to peak Hg concentrations in all sediment cores show near zero  $\Delta^{200}\text{Hg}$  (Fig. 5a) and  $\Delta^{204}\text{Hg}$  (Fig. 5b) values likely indicates dilution of atmospheric deposition of regional/global origin by local industrial inputs. Therefore, these ratios, in addition to  $^{206}\text{Pb}/^{204}\text{Pb}$  ratios at corresponding depths (Fig. 3d), are indicative of mining/smelting sources. The possibility that peak Hg and Pb concentrations originate from different sources was deemed unlikely, because Hg and Pb are highly correlated (Figs. S5 and S6), show strong temporal correspondence (Fig. 3), and are both known to be associated with mining and smelting operations (Ettler et al., 2006; Ma et al., 2013; Nriagu and Pacyna, 1988). Additionally, Great Salt Lake is a system previously documented to be impacted by mining and smelting activity (Wurtsbaugh et al., 2020).

In the Great Salt Lake system,  $\Delta^{199}\text{Hg}$  is a tracer of photochemical processing rather than a source tracer (Fig. 5c), because  $\Delta^{199}\text{Hg}$  varies with lake elevation (Fig. 5c) and is not correlated with Hg concentration or  $^{206}\text{Pb}/^{204}\text{Pb}$  ratios (Fig. 3). The fact that volume to area ratio (a proxy for average depth) for the south arm of Great Salt Lake fluctuates relatively little compared to overall lake stage (Fig. 5d) indicates the greater extent of shallow regions at higher lake levels, and by extension, a

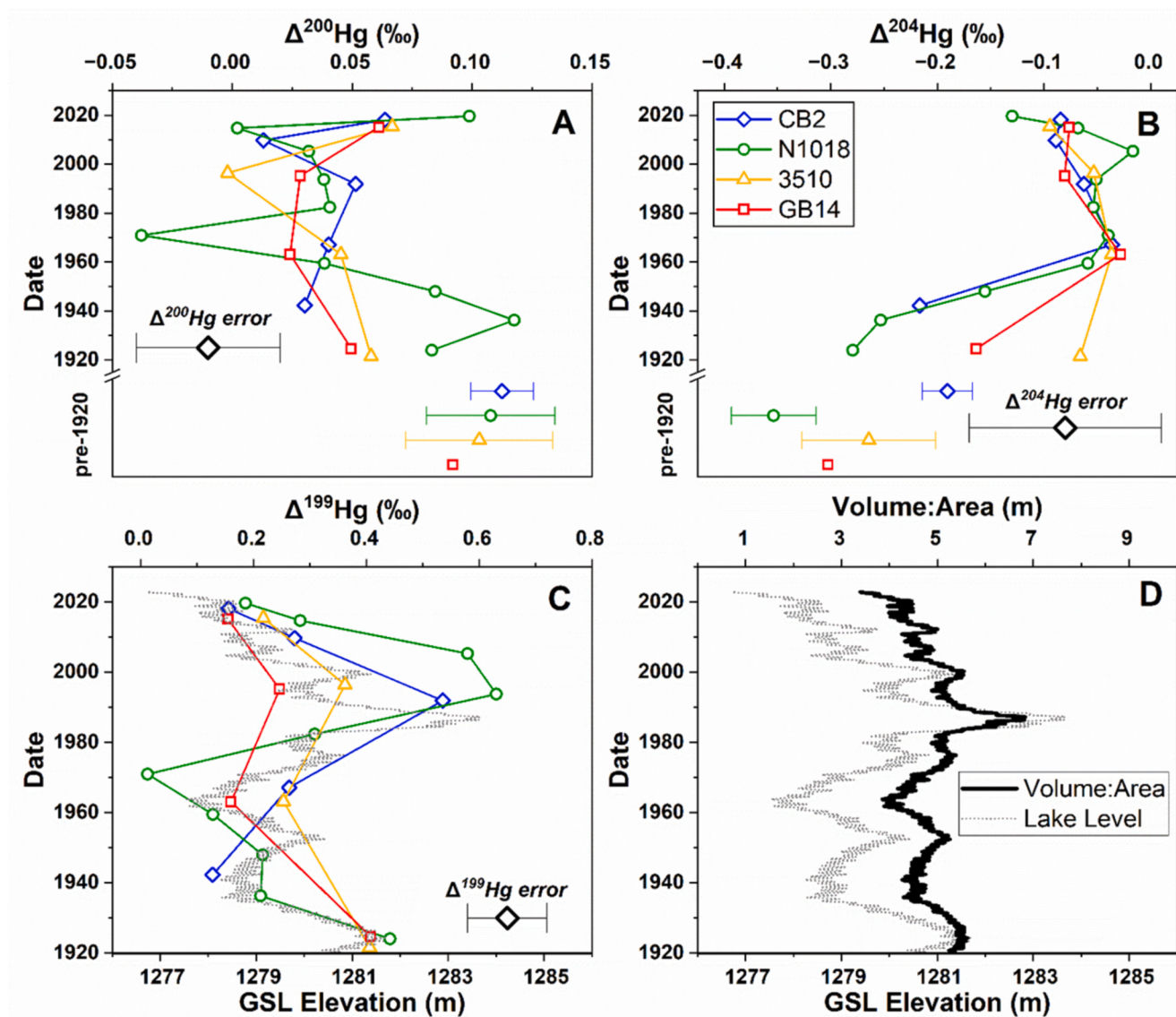


**Fig. 5.** a)  $\Delta^{200}\text{Hg}$ , b)  $\Delta^{204}\text{Hg}$ , and c)  $\Delta^{199}\text{Hg}$  measurements in four dated Great Salt Lake sediment cores. The black sample error symbol (inverted triangle) represents the 2 SD of measurements on IAEA 456 ( $n = 6$ ) for  $\Delta^{200}\text{Hg}$ ,  $\Delta^{204}\text{Hg}$ , and  $\Delta^{199}\text{Hg}$ . Error bars on pre-1920's background values for  $\Delta^{200}\text{Hg}$  and  $\Delta^{204}\text{Hg}$  represent the 1 SD of sample values associated with depths lacking measurable unsupported  $^{210}\text{Pb}$  (CB2:  $n = 8$ ; N1018:  $n = 5$ ; 3510:  $n = 5$ ; GB14:  $n = 7$ ). d) Volume to area ratios and lake level for the South Arm of Great Salt Lake as a function of date. Volume to area ratios are derived from Great Salt Lake bathymetric data (Root, 2023).

greater portion of the Great Salt Lake water column exposed to sunlight penetration and subsequent photochemical Hg loss. Although this study mainly examines changes in Hg sources over time, the  $\Delta^{199}\text{Hg}$  record demonstrates increased Hg photochemical processing during high water levels in the 1980s. This finding is consistent with MeHg demethylation being enhanced in surficial sediments underlying hypersaline open waters of Great Salt Lake relative to other (e.g., wetland) locations (Boyd et al., 2017).

### 3.3. Hg concentrations and stable isotope compositions of wet and dry deposition

To confirm the contributions of atmospheric deposition to sediments in Great Salt Lake, we further examined Hg concentrations and isotopes values in wet deposition and total gaseous mercury (TGM) from the region. Three rainfall samples collected adjacent to Great Salt Lake had Hg concentrations of 16, 11, and 1.4 ng/L, with the lowest concentration sample collected on the tail end of a multi-day rain event, consistent

with washout effects (Weiss-Penzias et al., 2016). Rainfall Hg concentrations are near the lower end of the range of values previously reported for Great Salt Lake (16.5 to 309.9 ng/L) (Naftz et al., 2009), and the three Great Salt Lake precipitation samples lacked sufficient volume and Hg mass to analyze for Hg stable isotopes. Therefore, we used literature values of two samples collected at locations in adjacent states near Jackson, WY ( $\delta^{202}\text{Hg} = -0.06 \text{\textperthousand}$ ,  $\Delta^{200}\text{Hg} = 0.23 \text{\textperthousand}$ ) and Steamboat Springs, CO ( $\delta^{202}\text{Hg} = 0.17 \text{\textperthousand}$ ,  $\Delta^{200}\text{Hg} = 0.23 \text{\textperthousand}$ ) (Fig. 6b) to represent the isotope values in rainfall (Kurz et al., 2019). Though published data on rainfall for the Rocky Mountain region are limited, these reference values are largely consistent with  $\Delta^{200}\text{Hg}$  values in precipitation samples collected globally (Chen et al., 2012; Demers et al., 2013; Enrico et al., 2016).

Isotope values for dry deposition were obtained from TGM samples ( $n = 3$ ) previously collected adjacent to Great Salt Lake ( $\delta^{202}\text{Hg} = 0.12 \pm 0.38 \text{\textperthousand}$ ,  $\Delta^{200}\text{Hg} = -0.08 \pm 0.02 \text{\textperthousand}$ ,  $n = 3$ ) (Fig. 6b) (Tate et al., 2023). Though the number of TGM samples is limited,  $\Delta^{200}\text{Hg}$  values are consistent with other TGM samples collected in the southwestern United

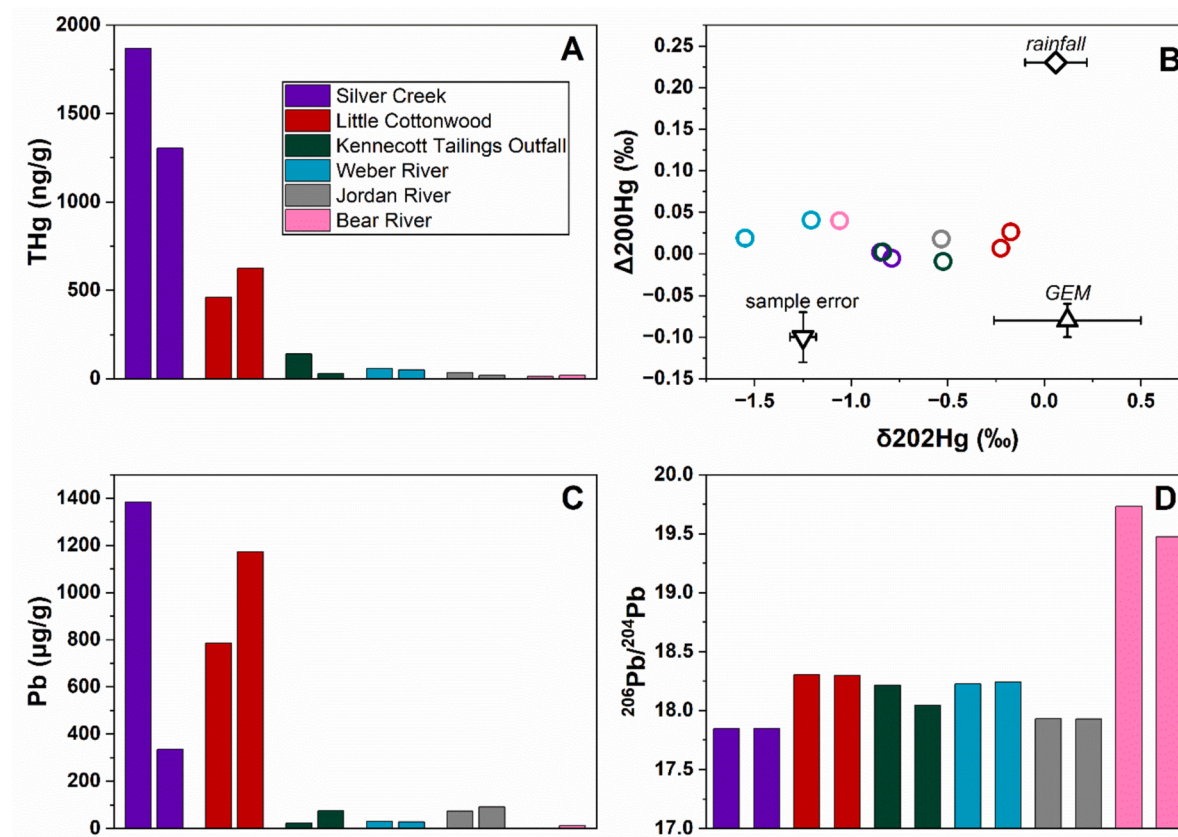


**Fig. 6.** a) Hg concentrations in tributary surficial sediment samples, b) Hg isotope biplot of  $\Delta^{200}\text{Hg}$  vs  $\delta^{202}\text{Hg}$  for tributary surficial sediment (circles), gaseous elemental Hg (GEM) (triangle), and rainfall (diamond) samples, c) Pb concentrations in tributary surficial sediment samples, and d)  $^{206}\text{Pb}/^{204}\text{Pb}$  isotope ratios in tributary surficial sediment samples. In panel b, the black sample error symbol (inverted triangle) represents the 2 SD of measurements on IAEA 456 ( $n = 6$ ) for  $\delta^{202}\text{Hg}$  and  $\Delta^{200}\text{Hg}$ . Error bars on GEM and rainfall samples represent the 1 SD ( $n = 3$  and  $n = 2$ , respectively).

States in Page, Arizona and El Paso, Texas ( $\delta^{202}\text{Hg} = 0.21 \pm 0.36 \text{ ‰}$ ,  $\Delta^{200}\text{Hg} = -0.08 \pm 0.03 \text{ ‰}$ ,  $n = 11$ ). The presence of positive  $\Delta^{200}\text{Hg}$  in wet deposition (precipitation) samples and negative  $\Delta^{200}\text{Hg}$  in dry deposition (TGM) samples is also consistent with Hg stable isotope values in wet and dry deposition samples collected globally (Chen et al., 2012; Demers et al., 2013; Kurz et al., 2019; Obrist et al., 2017; Tsui et al., 2020). With these atmospheric data, we are confident that the Hg isotope values in pre-industrial and contemporary sections of the Great Salt Lake cores are related to Hg from rainfall directly to the lake.

#### 3.4. Trace metal and isotope composition of tributary samples

To further assess contributions of watershed runoff to the Great Salt Lake cores, we conducted a small-scale assessment of sediments from Great Salt Lake tributaries across seven locations (two samples per location) (Fig. S1). These sediments displayed a wide range of Hg concentrations, ranging from  $16 \pm 5 \text{ ng/g}$  to  $1586 \pm 400 \text{ ng/g}$  (Fig. 6a). Surficial sediments with the highest Hg concentrations were collected from locations on Silver Creek ( $1586 \pm 400 \text{ ng/g}$ ,  $n = 2$ ) and Little Cottonwood Creek ( $543 \pm 17 \text{ ng/g}$ ,  $n = 2$ ), small headwater tributaries immediately downstream of historical mining activity (Fig. S1). Though Silver Creek and Little Cottonwood Creek eventually drain into the Weber and Jordan Rivers, respectively, downstream sediment samples collected at Weber and Jordan River sites were relatively low in Hg ( $53 \pm 4 \text{ ng/g}$ ,  $n = 2$ ;  $27 \pm 10 \text{ ng/g}$ ,  $n = 2$ ) (Fig. S1). Hg contributions to Great Salt Lake from high elevation, mining-impacted areas may have changed due to reservoir construction; for example, East Canyon Reservoir, a large reservoir located downstream of Silver Creek, was constructed between 1964 and 1966. Hg concentrations were relatively low in surficial sediment samples collected from the Bear and Weber

Rivers, which are primarily agriculturally dominated watersheds (Fig. S1). Mercury concentrations were also relatively low in Jordan River sediments despite the Jordan River flowing through the Wasatch Front Metropolitan Area for much of its length and the potential influence from mining impacted watersheds (e.g., Little Cottonwood Creek). Mercury concentrations in sediment samples collected from the Kennecott Tailings Outfall ( $84 \pm 79 \text{ ng/g}$ ,  $n = 2$ ) were lower than Hg concentrations of most recently deposited Great Salt Lake sediments in the four collected sediment cores ( $199 \pm 43 \text{ ng/g}$ ,  $n = 4$ ), suggesting that discharge from adjacent mine tailings may not be a substantial current source of Hg to Great Salt Lake, as has been established previously (Naftz et al., 2009).

Mercury stable isotope signatures in tributary surficial sediment samples displayed a gradient in  $\delta^{202}\text{Hg}$  values ( $-0.17$  to  $-1.55 \text{ ‰}$ ), with generally more depleted values in samples from tributaries less impacted by mining and urban inputs (Bear and Weber Rivers) and more enriched values in sites adjacent to mining and urban activity (Jordan River, Kennecott Tailings Outfall, Little Cottonwood Creek, and Silver Creek) (Fig. 6b). The negative  $\delta^{202}\text{Hg}$  values ( $-1.27 \text{ ‰} \pm 0.25$ ,  $n = 3$ ) in the Bear and Weber River sediment samples are consistent with negative values frequently observed in terrestrial runoff (Jiskra et al., 2017; Woerndle et al., 2018; Campeau et al., 2022), which has been attributed to foliar uptake of dry deposition, followed by sequestration in soils and subsequent erosion and watershed transport (Tsui et al., 2020). Though the mining impacted headwaters of Silver Creek eventually drain to the Weber River, the entire Weber River Basin has a relatively low density of mining sites, as does the Bear River Basin, and both basins have a relatively low proportion of urban land cover (Fig. S1). Therefore, Hg stable isotope signatures of sediments from the Bear and Weber Rivers (Fig. 6b) were used to derive a reference value for watershed inputs to

Great Salt Lake from non-urban, non-mining sources ( $\delta^{202}\text{Hg} = -1.27\% \pm 0.25\%$ ,  $\Delta^{200}\text{Hg} = +0.03\% \pm 0.01$ ,  $n = 3$ ).

Surficial sediment samples from sites adjacent to urban areas and mining activity had higher  $\delta^{202}\text{Hg}$  values (ranging from  $-0.20\% \pm 0.04$  at Little Cottonwood Creek to  $-0.82\% \pm 0.04$  at Silver Creek) relative to the watershed reference value. Additionally, all samples from urban/mining impacted sites were characterized by near zero even-MIF ( $\Delta^{200}\text{Hg} = 0.01 \pm 0.01\%$ ,  $n = 7$ ), consistent with expectations that mining/urban signatures would dilute contributions from atmospheric inputs of regional/global origin.

### 3.5. Hg and Pb pathways to Great Salt Lake

To further examine sources in Great Salt Lake sediments, we qualitatively compared Hg isotope data from sediment cores to representative atmospheric, industrial, and watershed endmembers. In order to directly compare atmospheric deposition data to Great Salt Lake sediment cores for  $\delta^{202}\text{Hg}$ , we had to account for an MDF shift of  $-0.4\%$  due to particle adsorption prior to sedimentation (Jiskra et al., 2012; Lepak et al., 2015). For the smelting (industrial) endmember, we did not have a representative sample within the watershed from active smelting or from current operating sites. The difficulty of obtaining representative ore samples for northern Utah mining/smelting operations throughout the 20th century required use of Pb concentrations and stable isotopes to estimate a mining/smelting endmember for Hg. Because Hg and Pb concentrations in all sediment cores show strong temporal correspondence (Fig. 3a and b) and correlation (Figs. S5 and S6), the Hg isotope endmember for mining/smelting was defined as the average isotope values of the sediment samples with the highest measured Pb concentration in each core ( $\delta^{202}\text{Hg} = -0.80\% \pm 0.08$ ,  $\Delta^{200}\text{Hg} = +0.03\% \pm 0.02$ ,  $n = 4$ ) on the basis that Pb stable isotope signatures at peak Pb concentrations reflect mining/smelting sources (Fig. 3d). We acknowledge the uncertainty in this estimated endmember particularly given our assumption that Hg from mining/smelting activities adjacent to Great Salt Lake are of similar isotopic composition. We justify this approach based on a sediment core from a Canadian smelting-contaminated lake in which  $\delta^{202}\text{Hg}$  values are largely constant throughout post-1930s sediments corresponding to the greatest period of contamination, and  $\delta^{202}\text{Hg}$  values associated with smelting contamination in this core ( $\delta^{202}\text{Hg} = -0.85 \pm 0.25$ ,  $n = 18$ ) (Ma et al., 2013) are similar to our derived mining/smelting endmember for Great Salt Lake ( $\delta^{202}\text{Hg} = -0.80\% \pm 0.08$ ,  $n = 4$ ).

As mentioned above, watershed sources ranged from  $-0.17$  to  $-1.55\%$  in  $\delta^{202}\text{Hg}$ , which, when compared to literature values (Tsui et al., 2020), range from industrially affected (e.g., mining) to reference values (e.g., atmospheric deposition). However, watershed inputs from non-mining/smelting sources likely do not significantly contribute to the lower  $\delta^{202}\text{Hg}$  values in 1950–2000 sediments based on the fact that concentrations of aluminum (Al) (Fig. S7), a conservative tracer of lithogenic material erosion within watersheds (Engstrom and Wright, 1984; Wurtsbaugh et al., 2020), are relatively constant in Great Salt Lake sediments except for reduced values in the top 2–4 cm. Thus, watershed erosion alone (without consideration of mining impacts) cannot account for the 15- to 25-fold increase in Hg concentrations from pre-1920 background to peak values (Fig. 3a). Lead isotope signatures in surficial sediments from the Bear River (Fig. 6d), which has limited upstream mining activity, are similar to pre-1920 background values in all Great Salt Lake sediment cores. Lead isotope signatures in surficial sediments from all other tributaries, which have greater upstream mining activity and are proximal to current and historic smelting operations, are similar to post-1920 values in Great Salt Lake sediment cores. Therefore, the increase in Pb and Hg concentrations within Great Salt Lake sediment cores is likely driven by an increase in mining/smelting source contributions, either through local airborne emissions or downstream transport within mining-impacted tributaries.

In pre-1920 and present-day sediments, the lack of depleted  $\delta^{202}\text{Hg}$

values (Fig. 3b) suggests minimal contribution of watershed (terrestrial runoff) Hg inputs, which were also independently estimated to comprise approximately 15 % of current annual Hg loads to Great Salt Lake based on measured Hg concentration values (Naftz et al., 2009). Particulate matter from watershed sources are not expected to contribute significantly to Great Salt Lake sediments in open water environments, where sedimentation is dominated by brine shrimp and algal settling and decomposition (Maszczyk and Wurtsbaugh, 2017). Enriched  $\delta^{202}\text{Hg}$  values in present day sediments are likely not due to increased urban/mining sourced Hg in watershed inputs, because the lack of even MIF in surficial sediments collected from urban/mining impacted Great Salt Lake tributaries ( $\Delta^{200}\text{Hg} = 0.01 \pm 0.01\%$ ,  $n = 7$ ) does not correspond with the positive even MIF observed in present day Great Salt Lake sediments ( $\Delta^{200}\text{Hg} = 0.07 \pm 0.02\%$ ,  $n = 4$ ) attributed to precipitation delivery of Hg.

Thus, Hg source attribution in Great Salt Lake sediments can be explained by a combination of two isotope tracers ( $\delta^{202}\text{Hg}$  and  $\Delta^{200}\text{Hg}$ ), wherein a smelting endmember signature ( $\delta^{202}\text{Hg} = -0.80\% \pm 0.08$ ,  $\Delta^{200}\text{Hg} = +0.03\% \pm 0.02$ ) contrasts with atmospheric deposition endmembers (dry deposition:  $\delta^{202}\text{Hg} = -0.28 \pm 0.38\%$ ,  $\Delta^{200}\text{Hg} = -0.08 \pm 0.02\%$ ; wet deposition:  $\delta^{202}\text{Hg} = -0.34\% \pm 0.16$ ,  $\Delta^{200}\text{Hg} = 0.23 \pm 0.00\%$ ) (Fig. 7). Though we chose not to use a quantitative analysis of source contributions in each Great Salt Lake sediment core section, sediment samples from the four cores are adequately encompassed by atmospheric and mining/smelting endmembers (Fig. 7), with pre-1920 and present-day sediment values falling between dry and wet deposition endmembers, and 1950–2000 values closer to the mining/smelting endmember. Pre-1920 and present day sediment values falling between wet and dry atmospheric deposition endmembers (Fig. 7) is consistent with previous studies documenting approximately equivalent wet and dry atmospheric contributions to Great Salt Lake based on measured and estimated loads (Naftz et al., 2009; Peterson and Gustin, 2008).

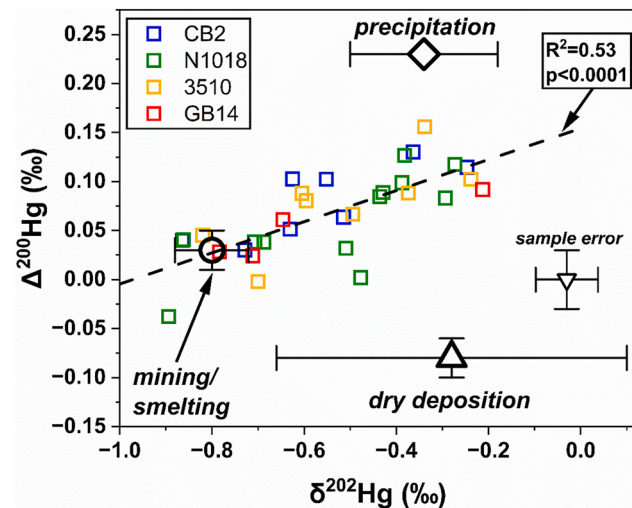


**Fig. 7.** Hg isotope biplot of  $\Delta^{200}\text{Hg}$  vs  $\delta^{202}\text{Hg}$  measurements in sediment cores collected from sites CB2, N1018, 3510, and GB14 (blue, green, yellow, and red squares, respectively). The sample error (inverted triangle) represents the 2 SD of measurements on IAEA 456 ( $n = 6$ ) for  $\delta^{202}\text{Hg}$  and  $\Delta^{200}\text{Hg}$ . Error bars on dry deposition, precipitation, and mining/smelting endmembers (large black symbols) represent the 1 SD of measurements ( $n = 3$ ,  $n = 2$ , and  $n = 4$ , respectively) used to estimate endmember values. The wet deposition endmember was derived using values from two precipitation samples collected near Jackson, WY and Steamboat Springs, CO (Kurz et al., 2019), and the dry deposition endmember was derived from values of the gaseous elemental Hg (GEM) samples previously collected adjacent to Great Salt Lake (Tate et al., 2023). An MDF shift of  $-0.4\%$  due to particle adsorption prior to sedimentation was applied to atmospheric deposition data to allow for direct comparison to Hg isotope data from sediment cores (Jiskra et al., 2012; Lepak et al., 2015).

We propose that Hg contributions to Great Salt Lake during periods corresponding to peak sediment Hg concentrations were primarily associated with local airborne emissions from mining and smelting operations. Associated Hg stable isotope signatures ( $\delta^{202}\text{Hg}$ ) being generally isotopically lighter than pre-1920s background values (Fig. 3c) is consistent with expectations of an isotopically lighter combustion product based on principles of MDF. Because these local emissions likely did not undergo long range atmospheric transport prior to deposition (and were therefore not subject to photochemical oxidation in the upper atmosphere), they exhibit little even-MIF ( $\Delta^{200}\text{Hg}$  and  $\Delta^{204}\text{Hg}$ ) compared to atmospheric inputs of regional/global origin (Fig. 5). This is consistent with observations of TGM isotope signatures near Oak Ridge, Tennessee, where local emission sources are dominant and minimal even-MIF is observed compared to other sites throughout the United States (Tate et al., 2023). Although Hg contributions from mining-impacted Great Salt Lake tributaries or contributions from documented tailings pond breaches or leaks (Waddell et al., 2009; Wurtsbaugh et al., 2020) cannot be entirely ruled out, the correspondence of peak Hg concentrations to the closure of multiple smelting operations and the construction of a taller 370 m stack at the Garfield Smelter with better emission controls (Wurtsbaugh et al., 2020), along with the rapid rebound in Hg concentrations and isotope signatures towards present-day values (Fig. 3), likely indicates declines in local atmospheric Hg emissions. Peak source contributions tied to larger intact pools of Hg (such as mining-impacted soils in upstream tributaries) would likely lead to slower ecological turnover times than those observed at Great Salt Lake, and current tributary contributions of Hg to the lake are low relative to atmospheric inputs (Naftz et al., 2009). Additionally, Hg concentrations in sediment samples collected from the Bear, Weber, and Jordan Rivers near their terminus with Great Salt Lake are low relative to those in both mid-20th century and most recently deposited Great Salt Lake sediments (Figs. 3a and 6a), further suggesting that watershed contributions from upstream mining activities are low.

Present day relative to background (pre-1920) isotope signatures in sediment are similar for Hg (Fig. 3c) but dissimilar for Pb (Fig. 3d), likely indicating differences in relative magnitudes of current source contributions or in-lake processing. These differences are due to the more complex biogeochemical cycle and transport pathways for Hg relative to those of Pb. Minimal rebound in Pb isotope signatures in present day sediments despite decreasing Pb concentrations (Fig. 3b and d) indicate that mining and smelting inputs, though reduced, are likely still the predominant source of Pb to Great Salt Lake. In contrast, the more pronounced rebound in Hg stable isotope values (Figs. 3d, 5a, and b) indicates a shift from local mining/smelting sources to greater contributions of atmospheric inputs of regional or global origin. The fact that Hg concentrations have not decreased to pre-1920 levels (Fig. 3a) is consistent with globally increased atmospheric Hg deposition by a factor of three since pre-industrial times (Driscoll et al., 2013), but could also indicate ongoing recovery of the Great Salt Lake system to contamination from local mining/smelting sources.

### 3.6. Other trace metals

Temporal correspondence and correlation of other trace metals (e.g., Cu, Sb, Cd, Zn, Se, Mo, Tl) with Pb concentrations and stable isotope ratios (Figs. 4, S5, and S7) also implies that peak concentrations of other metals in Great Salt Lake sediments are sourced from mining/smelting activity, as has been suggested in a previous study (Wurtsbaugh et al., 2020). Although metals such as Cu, Sb, and Zn are lower in present day sediments relative to peak values (Fig. 4), other trace elements, including Se, have not exhibited recent declines (Fig. S7), consistent with analyses of other Great Salt Lake sediment cores (Wurtsbaugh et al., 2020). Selenium is elevated in both the main body and wetlands of Great Salt Lake (Diaz et al., 2009; Dicataldo et al., 2011) and is a contaminant of concern for Great Salt Lake due to risk to migratory birds (Ohlendorf et al., 2009). The onset of increasing Se concentrations temporally

corresponds to shifts in Pb and Hg concentration and stable isotope measurements (Fig. 3) and indicates a likely mining/smelting source; however, it is unclear whether additional sources are contributing to the elevated values in most recently deposited sediments. A characterization of Se loads entering the south arm of Great Salt Lake revealed the potential for uncharacterized loads (Diaz et al., 2009). One likely but relatively uncharacterized source of Se to Great Salt Lake is legacy contamination associated with metal refining and smelting operations near the south shore. Waste from these operations was previously stored in unlined lagoons, and associated contaminant plumes infiltrated and intersected a groundwater system supplying a wetland complex on the south shore of Great Salt Lake (Waddell et al., 2009). Sediment chronologies in this and other studies (Oliver et al., 2009; Wurtsbaugh et al., 2020) have relatively low temporal resolution, so dataset interpretation from routine USGS and Utah Department of Environmental Quality biannual monitoring over the past two decades could help better characterize recent spatial and temporal trends with respect to Se at Great Salt Lake. Additionally, greater characterization of current Se inputs from legacy mining/smelting waste could inform management strategies to protect bird habitat at Great Salt Lake.

Elevated trace metal concentrations in Great Salt Lake sediments generally occur within the top 12 cm of Great Salt Lake sediments (Fig. S8), indicating that if lake surface area, which has already decreased from baseline by >50 % (Null and Wurtsbaugh, 2020), continues to decline, sediments with the highest trace metal concentrations are likely to be the first to be eroded and entrained in the atmosphere as dust by strong winds. These findings are consistent with those of another study (Perry et al., 2019) which found that surface sediments and dust eroded from the Great Salt Lake lakebed contain elevated levels of trace metals such as As, Co, Pb, Cr, Cd, Tl, Cu, and Zn. Some trace elements, including Co, Cu, Sb, and As, have levels in the PM<sub>10</sub> fraction of playa material that exceed residential and/or industrial risk-specific levels established by the U.S. EPA (Perry et al., 2019). In cases where peak trace metals in concentrations occur at depths below the surficial level (e.g., >1 cm), as is the case for several trace metals analyzed in this study (Figs. 2 and 3), wind erosion of the top layers of playa could result in further mobilization of dust containing higher trace metal concentrations sourced from mining and smelting activities and potential airborne health risk to ecosystem health in areas adjacent to Great Salt Lake. However, sediment cores in this study were generally collected from deeper environments (>4 m) and were not collected from near shoreline areas that may have different trace metal concentration distributions. This includes the eastern margins and wetland environments that may be impacted by additional metal sources (such as wastewater treatment plant or industrial effluent) (Waddell et al., 2009; Wurtsbaugh et al., 2020). Further study would be needed to determine trace metal sources and concentrations in sediments near shoreline areas that would be the first to be exposed following additional declines in lake level.

## 4. Conclusion

This study used Hg and Pb stable isotope measurements to directly assess current and historic sources of Hg, Pb, and other trace metals accumulating in Great Salt Lake sediments. To our knowledge, this is the first study to use stable isotope tracers to examine metal contaminant sources at Great Salt Lake. The coupled use of Hg and Pb stable isotopes in this study, in addition to metal concentration measurements, provides an example of how multiple metal isotope ratios can be used as a tool for pollution source attribution. Lead isotopes were used to assess relative contributions of mining/smelting sources for Hg (and other metals) to the Great Salt Lake system. The correspondence of Pb isotopes in sediments to ores mined and smelted in the vicinity of Great Salt Lake indicates that mining/smelting is likely a primary contributor of Pb to Great Salt Lake throughout much of the 20th century and present day. Correlation of Hg and Pb concentrations and stable isotope signatures indicates local mining/smelting as a source of Hg to the system. Mercury

isotope signatures provided additional information about sources and pathways not described by Pb isotope signatures such as diverging source pathways for Hg (regional/global atmospheric) and Pb (local mining/smelting) to the present environment.

Increased contributions of regional/global sources in present day sediments determined using Hg stable isotopes indicate Hg contributions from local industrial sources may not drive the elevated MeHg concentrations observed currently in the water column and biota of Great Salt Lake. Instead, Hg bioaccumulation at Great Salt Lake may be driven by enhanced MeHg production within the system, which is strongly implied by anoxic, sulfate reducing, and organic rich conditions documented in deep water and sediment environments at Great Salt Lake, coupled with elevated MeHg concentrations exceeding 30 ng/L (Naftz et al., 2008; Valdes et al., 2017; Yang et al., 2019). Contributions of primarily regional/global Hg sources to the present day environment is consistent with a previous study that documented that atmospheric Hg concentrations were comparable to global background values and found no obvious specific local Hg sources to Great Salt Lake using back trajectory analysis, concluding that atmospheric inputs of Hg directly to Great Salt Lake may be sufficient to account for contemporary Hg concentrations in brine shrimp (Peterson and Gustin, 2008). If atmospheric inputs from sources of regional and global origin are dominant, further declines in Hg inputs from local sources may not lead to proportionate declines in Hg concentrations in biota. Further mitigating Hg in the open water environments of Great Salt Lake is likely more dependent on national and global reductions in Hg emissions and management strategies designed to limit MeHg production at bioaccumulation hotspots within the system. However, Hg source profiles may differ for eastern wetland regions of Great Salt Lake, which may be more influenced by tributary inflows and local industrial sources from the adjacent Wasatch Front Metropolitan Area. Eastern lake margins and wetland areas provide important habitat for waterfowl and are current sources of dust emissions, but further study would be needed to determine additional sources of trace metal contamination within these areas.

Although most trace metal concentrations in sediment are lower in recently deposited sediments relative to those deposited in the mid-20th century, some elements, such as Se, remain elevated, which may pose a threat to migratory birds. As discussed previously, current inputs may be comprised of under-characterized legacy sources, such as Se from improper waste management at sites associated with mining/smelting operations, particularly at the southern end of Great Salt Lake. Greater characterization of these Se sources could help inform management strategies for protecting bird habitat. Generally, the highest trace metal concentrations in Great Salt Lake sediments are linked to mining and smelting sources, are enriched in the top 12 cm of sediments, and could be mobilized during wind events if long term trends of declining lake levels and lake bed desiccation continue. However, risk assessment of airborne contaminants in dust mobilized from the Great Salt Lake playa is beyond the scope of this study. Though addressing these knowledge gaps is still needed, this study contributes to our understanding of historical changes in Hg and trace metal sources to Great Salt Lake, a key ecosystem of hemispheric importance for waterfowl. Furthermore, this study demonstrates the utility of using multiple stable isotope systems (Hg and Pb) to investigate both sources and pathways of trace metals to the Great Salt Lake system, a concept that can extend to metal source tracking studies in other systems.

## Funding

This work was supported by the National Science Foundation (Grant #2229765), the University of Utah Global Change and Sustainability Center, FRIENDS of Great Salt Lake, and U.S. Geological Survey Environmental Health-Toxic Substances Hydrology Program. Any use of trade, firm, or product names is for descriptive purposes only and does not imply endorsement by the U.S. Government.

## CRediT authorship contribution statement

**Samuel F. Lopez:** Writing – original draft, Visualization, Investigation, Formal analysis, Conceptualization. **Sarah E. Janssen:** Writing – original draft, Visualization, Investigation, Formal analysis, Conceptualization. **Michael T. Tate:** Investigation, Formal analysis. **Diego P. Fernandez:** Writing – review & editing, Formal analysis. **Christopher R. Anderson:** Formal analysis. **Grace J. Armstrong:** Formal analysis. **Thomas C. Wang:** Formal analysis. **William P. Johnson:** Writing – review & editing, Writing – original draft, Supervision, Resources, Project administration, Methodology, Investigation, Conceptualization.

## Declaration of competing interest

The authors declare that they have no known competing financial interests or personal relationships that could have appeared to influence the work reported in this paper.

## Acknowledgements

We gratefully acknowledge several USGS Utah Water Science Center staff that aided in field sampling efforts. We would also like to specifically acknowledge Ashley Fenwick, Bryan Bielicki, Kevin Engberson, and Mac Borrowman for their assistance with tributary sediment collection. We also thank the staff of the USGS MRL for their support with sample analysis and data management. We are grateful to Adam Heathcote and Erin Mortenson at the St. Croix Watershed Research station for their expertise in Pb-210 dating of sediment cores.

## Appendix A. Supplementary data

Supplementary data to this article can be found online at <https://doi.org/10.1016/j.scitotenv.2024.177374>.

## Data availability

Data will be made available on request.

## References

- Aldrich, T.W., Paul, D.S., 2002. Avian ecology of Great Salt Lake. In: Gwynn, J.W. (Ed.), *Great Salt Lake: An Overview of Change*. Utah Geological Survey, Salt Lake City, Utah, USA, pp. 343–374.
- Appleby, P.G., Oldfield, F., 1992. Application of 210Pb to sedimentation studies. In: Ivanovich, M., Haromon, R.S. (Eds.), *Uranium-series Disequilibrium: Application to Earth, Marine, and Environmental Sciences*. Clarendon Press, Oxford.
- Baskin, R.L., 2005. Calculation of Area and Volume for the South Part of Great Salt Lake, Utah. <https://doi.org/10.3133/ofr20051327>.
- Beisner, K., Naftz, D.L., Johnson, W.P., Diaz, X., 2009. Selenium and trace element mobility affected by periodic displacement of stratification in the Great Salt Lake, Utah. *Sci Total Environ* 407 (19), 5263–5273. <https://doi.org/10.1016/j.scitotenv.2009.06.005>.
- Bergquist, B.A., Blum, J.D., 2007. Mass-dependent and -independent fractionation of hg isotopes by photoreduction in aquatic systems. *Science* 318 (5849), 417–420. <https://doi.org/10.1126/science.1148050>.
- Blum, J.D., Bergquist, B.A., 2007. Reporting of variations in the natural isotopic composition of mercury. *Anal Bioanal Chem*. 388 (2), 353–359. <https://doi.org/10.1007/s00216-007-1236-9>.
- Blum, J.D., Johnson, M.W., 2017. Recent developments in mercury stable isotope analysis. *Rev Mineral Geochem*. 82 (1), 733–757. <https://doi.org/10.2138/rmg.2017.82.17>.
- Boyd, E.S., Yu, R.Q., Barkay, T., Hamilton, T.L., Baxter, B.K., Naftz, D.L., Marvin-DiPasquale, M., 2017. Effect of salinity on mercury methylating benthic microbes and their activities in Great Salt Lake, Utah. *Sci. Total Environ.* 581–582, 495–506. <https://doi.org/10.1016/j.scitotenv.2016.12.157>.
- Campeau, A., Eklöf, K., Soerensen, A.L., Åkerblom, S., Yuan, S., Hintelmann, H., Bieroza, M., Köhler, S., Zdanowicz, C., 2022. Sources of riverine mercury across the Mackenzie River Basin; inferences from a combined Hg C isotopes and optical properties approach. *Sci. Total Environ.* 806 (4), 150808. <https://doi.org/10.1016/j.scitotenv.2021.150808>.
- Chen, J., Hintelmann, H., Feng, X., Dimock, B., 2012. Unusual fractionation of both odd and even mercury isotopes in precipitation from Peterborough, ON, Canada. *Geochim. Cosmochim. Acta* 90, 33–46. <https://doi.org/10.1016/j.gca.2012.05.005>.

- Chow, T.J., Earl, J.L., 1972. Lead isotopes in North American coals. *Science* 176 (4034), 510–511. <https://doi.org/10.1126/science.176.4034.510>.
- Conover, M.R., Bell, M.E., 2020. Importance of Great Salt Lake to pelagic birds: eared grebes, phalaropes, gulls, ducks, and white pelicans. In: Baxter, B.K., Butler, J.K. (Eds.), *Great Salt Lake Biology: A Terminal Lake in a Time of Change*. Springer, pp. 239–262.
- Demers, J.D., Blum, J.D., Zak, D.R., 2013. Mercury isotopes in a forested ecosystem: implications for air-surface exchange dynamics and the global mercury cycle. *Global Biogeochem. Cycles* 27 (1), 222–238. <https://doi.org/10.1002/gbc.20021>.
- Diaz, X., Johnson, W.P., Naftz, D.L., 2009. Selenium mass balance in the Great Salt Lake, Utah. *Sci Total Environ* 407 (7), 2333–2341. <https://doi.org/10.1016/j.scitotenv.2008.11.029>.
- Dicataldo, G., Johnson, W.P., Naftz, D.L., Hayes, D.F., Moellmer, W.O., Miller, T., 2011. Diel variation of selenium and arsenic in a wetland of the Great Salt Lake, Utah. *Applied Geochemistry* 26 (1), 28–36. <https://doi.org/10.1016/j.apgeochem.2010.10.011>.
- Driscoll, C.T., Mason, R.P., Chan, H.M., Jacob, D.J., Pirrone, N., 2013. Mercury as a global pollutant: sources, pathways, and effects. *Environ. Sci. Technol.* 47 (10), 4967–4983. <https://doi.org/10.1021/es305071v>.
- Engstrom, D.R., Wright, J.H.E., 1984. Chemical stratigraphic of lake sediments as a record of environmental change. In: Haworth, E.Y., Lund, J.W.G. (Eds.), *Lake Sediments and Environmental History*. University of Leicester Press, Leicester, pp. 11–67.
- Enrico, M., Roux, G.L., Maruszak, N., Heimbürger, L.E., Claustres, A., Fu, X., Sun, R., Sonke, J.E., 2016. Atmospheric mercury transfer to peat bogs dominated by gaseous elemental mercury dry deposition. *Environ. Sci. Technol.* 50 (5), 2405–2412. <https://doi.org/10.1021/acs.est.5b06058>.
- Etter, V., Mihaljevic, M., Sebek, O., Molek, M., Grygar, T., Zeman, J., 2006. Geochemical and Pb isotopic evidence for sources and dispersal of metal contamination in stream sediments from the mining and smelting district of Příbram, Czech Republic. *Environ. Pollut* 142 (3), 409–417. <https://doi.org/10.1016/j.envpol.2005.10.024>.
- Flavelle, C., 2022. As the Great Salt Lake Dries Up, Utah Faces an 'Environmental Nuclear Bomb'. *The New York Times*, 7 June 2022. Available at: <https://www.nytimes.com/2022/06/07/climate/salt-lake-city-climate-disaster.html>.
- Great Salt Lake Ecosystem Program, 2023. An Avain Oasis. <https://wildlife.utah.gov/gslep/wildlife/birds.html>. (Accessed 22 November 2023).
- Janssen, S.E., Lepak, R.F., Tate, M.T., Ogorek, J.M., DeWild, J.F., Babiarz, C.L., Hurley, J.P., Krabbenhoft, D.P., 2019. Rapid pre-concentration of mercury in solids and water for isotopic analysis. *Anal. Chim. Acta* 1054, 95–103. <https://doi.org/10.1016/j.aca.2018.12.026>.
- Janssen, S.E., Hoffman, J.C., Lepak, R.F., Krabbenhoft, D.P., Walters, D., Eagles-Smith, C.A., Peterson, G., Ogorek, J.M., DeWild, J.F., Cotter, A., Pearson, M., Tate, M.T., Yearndle Jr., R.B., Mills, M.A., 2021. Examining historical mercury sources in the Saint Louis River estuary: how legacy contamination influences biological mercury levels in Great Lakes coastal regions. *Sci. Total Environ.* 779, 146284. <https://doi.org/10.1016/j.scitotenv.2021.146284>.
- Jewell, P.W., 2021. Historic low stand of Great Salt Lake, Utah: I. SN Appl. Sci. 3 (8). <https://doi.org/10.1007/s42452-021-04691-5>.
- Jiskra, M., Wiederhold, J.G., Bourdon, B., Kretschmar, R., 2012. Solution speciation controls mercury isotope fractionation of Hg(II) sorption to goethite. *Environ. Sci. Technol.* 46 (12), 6654–6662. <https://doi.org/10.1021/es3008112>.
- Jiskra, M., Wiederhold, J.G., Skjellberg, U., Kronberg, R., Kretschmar, R., 2017. Source tracing of natural organic matter bound mercury in boreal forest runoff with mercury stable isotopes. *Environ. Sci.: Processes Impacts* 19, 1235–1248. <https://doi.org/10.1039/C7EM00245A>.
- Johnson, W.P., Swanson, N., Black, B., Rudd, A., Carling, G., Fernandez, D.P., Luft, J., Van Leeuwen, J., Marvin-DiPasquale, M., 2015. Total- and methyl-mercury concentrations and methylation rates across the freshwater to hypersaline continuum of the Great Salt Lake, Utah, USA. *Sci. Total Environ.* 511, 489–500. <https://doi.org/10.1016/j.scitotenv.2014.12.092>.
- Kurz, A.Y., Blum, J.D., Washburn, S.J., Baskaran, M., 2019. Changes in the mercury isotopic composition of sediments from a remote alpine lake in Wyoming, USA. *Sci. Total Environ.* 669, 973–982. <https://doi.org/10.1016/j.scitotenv.2019.03.165>.
- Lepak, R.F., Yin, R., Krabbenhoft, D.P., Ogorek, J.M., DeWild, J.F., Holsen, T.M., Hurley, J.P., 2015. Use of stable isotope signatures to determine mercury sources in the Great Lakes. *Environ. Sci. Technol. Lett.* 2 (12), 335–341. <https://doi.org/10.1021/acs.estlett.5b00277>.
- Lopez, S.F., Janssen, S.E., Tate, M.T., Fernandez, D.P., Poulin, B.A., Black, F.J., Johnson, W.P., 2024. Assessment of Mercury, Mercury Stable Isotopes, and Trace Metals in Waters, Sediments, and Biota From Great Salt Lake, Utah. U.S. Geological Survey data release. <https://doi.org/10.5066/P13XSQWN>.
- Ma, J., Hintelman, H., Kirk, J.L., Muir, D.C.G., 2013. Mercury concentrations and mercury isotope composition in lake sediment cores from the vicinity of a metal smelting facility in Flin Flon, Manitoba. *Chem. Geol.* 336, 96–102. <https://doi.org/10.1016/j.chemgeo.2012.10.037>.
- Maszczynski, P., Wurtzbaugh, W.A., 2017. Brine shrimp grazing and fecal production increase sedimentation to the deep brine layer (monimolimnion) of Great Salt Lake, Utah. *Hydrobiologia* 802 (1), 7–22. <https://doi.org/10.1007/s10750-017-3235-y>.
- Monna, F., Hamer, K., Lévéque, J., Sauer, M., 2000. Pb isotopes as a reliable marker of early mining and smelting in the Northern Harz province (Lower Saxony, Germany). *J. Geochem. Explor.* 68 (3), 201–210. [https://doi.org/10.1016/s0375-6742\(00\)00005-4](https://doi.org/10.1016/s0375-6742(00)00005-4).
- Naftz, D., Angeroth, C., Kenney, T., Waddell, B., Darnall, N., Silva, S., Perschon, C., Whitehead, J., 2008. Anthropogenic influences on the input and biogeochemical cycling of nutrients and mercury in Great Salt Lake, Utah, USA. *Appl. Geochem.* 23 (6), 1731–1744. <https://doi.org/10.1016/j.apgeochem.2008.03.002>.
- Naftz, D., Fuller, C., Cederberg, J., Krabbenhoft, D., Whitehead, J., Gardberg, J., Beisner, K., 2009. Mercury inputs to Great Salt Lake, Utah: Reconnaissance-Phase results. *Natural Resources and Environmental Issues* 15.
- Nelson, S.J., Willacker, J., Eagles-Smith, C., Flanagan Pritz, C., Chen, C.Y., Klemmer, A., Krabbenhoft, D.P., 2024. Habitat and dissolved organic carbon modulate variation in the biogeochemical drivers of mercury bioaccumulation in dragonfly larvae at the national scale. *Sci. Total Environ.* 912, 169396. <https://doi.org/10.1016/j.scitotenv.2023.169396>.
- Nriagu, J.O., Pacyna, J.M., 1988. Quantitative assessment of worldwide contamination of air, water and soils by trace metals. *Nature* 333 (6169), 134–139. <https://doi.org/10.1038/333134a0>.
- Null, S.E., Wurtzbaugh, W.A., 2020. Water development, consumptive water uses, and Great Salt Lake. In: Baxter, B.K., Butler, J.K. (Eds.), *Great Salt Lake Biology: A Terminal Lake in a Time of Change*. Springer, pp. 1–23. [https://doi.org/10.1007/978-3-030-40352-2\\_1](https://doi.org/10.1007/978-3-030-40352-2_1).
- Obrist, D., Agnani, Y., Jiskra, M., Olson, C.L., Colegrove, D.P., Hueber, J., Moore, C.W., Sonke, J.E., Helming, D., 2017. Tundra uptake of atmospheric elemental mercury drives Arctic mercury pollution. *Nature* 547 (7662), 201–204. <https://doi.org/10.1038/nature22997>.
- Ohlendorf, H.M., DenBleyker, J., Moellmer, W.O., Miller, T., 2009. Development of a site-specific standard for selenium in open waters of Great Salt Lake, Utah. *Natural Resources and Environmental Issues* 15 (1).
- Oliver, W., Fuller, C., Naftz, D.L., Diaz, X., 2009. Estimating selenium removal by sedimentation from the Great Salt Lake, Utah. *Applied Geochemistry* 24 (5), 936–949. <https://doi.org/10.1016/j.apgeochem.2009.02.023>.
- Perry, K.D., Crosman, E.T., Hoch, S.W., 2019. Results of the Great Salt Lake Dust Plume Study (2016–2018). In: Report to the Utah Division of Forestry, Fire, and State Lands.
- Peterson, C., Gustin, M., 2008. Mercury in the air, water and biota at the Great Salt Lake (Utah, USA). *Sci. Total Environ.* 405 (1–3), 255–268. <https://doi.org/10.1016/j.scitotenv.2008.06.046>.
- Putman, A.L., Blakowski, M.A., McDonnell, M.C., Diviesti, D.N., Fernandez, D.P., Longley, P.C., Jones, D., 2023. Assessing exposure of northern Utah communities to dust from the contaminated and dynamic Great Salt Lake playa. In: Report to the Utah Division of Forestry, Fire, and State Lands.
- Reynolds, R.L., Mordecai, J.S., Rosenbaum, J.G., Ketterer, M.E., Walsh, M.K., Moser, K.A., 2009. Compositional changes in sediments of subalpine lakes, Uinta Mountains (Utah): evidence for the effects of human activity on atmospheric dust inputs. *J. Paleolimnol.* 44 (1), 161–175. <https://doi.org/10.1007/s10933-009-9394-8>.
- Root, J.C., 2023. Half-meter topobathymetric elevation model and elevation-area-volume tables for Great Salt Lake, Utah, 2002–2016: U.S. Geological Survey data release, doi:<https://doi.org/10.5066/P9DGG75W>.
- Scholl, D., Ball, R., 2005. An Evaluation of Mercury Concentrations in Waterfowl from the Great Salt Lake, Utah for 2004 and 2005. Utah Department of Health, Office of Epidemiology, Environmental Epidemiology Program, Salt Lake City, Utah, USA.
- Scholl, D., Ball, R., 2006. An Evaluation of Mercury Concentrations in Waterfowl From the Great Salt Lake, Utah for 2005 and 2006. Utah Department of Health, Office of Epidemiology, Environmental Epidemiology Program, Salt Lake City, Utah, USA.
- Shiel, A.E., Weis, D., Orians, K.J., 2010. Evaluation of zinc, cadmium and lead isotope fractionation during smelting and refining. *Sci. Total Environ.* 408 (11), 2357–2368. <https://doi.org/10.1016/j.scitotenv.2010.02.016>.
- Stacey, J.S., Zartman, R.E., Nkomo, I.T., 1968. A lead isotope study of galenas and selected feldspars from mining districts in Utah. *Econ. Geol.* 63 (7), 796–814. <https://doi.org/10.2113/gsecongeo.63.7.796>.
- Tate, M.T., Janssen, S.E., Lepak, R.F., Flucke, L., Krabbenhoft, D.P., 2023. National-scale assessment of total gaseous mercury isotopes across the United States. *J. Geophys. Res. Atmos.* 128 (8), 1–15. <https://doi.org/10.1029/2022JD038276>.
- Tempest Williams, T., 2023. I am Haunted by What I have Seen at Great Salt Lake. The New York Times, 25 March 2023. Available at: <https://www.sltrib.com/opinion/commentary/2023/03/25/terry-tempest-williams-i-am/>.
- Teutsch, N., Erel, Y., Halicz, L., Banin, A., 2001. Distribution of natural and anthropogenic lead in Mediterranean soils. *Geochim. Cosmochim. Acta* 65 (17), 2853–2864. [https://doi.org/10.1016/s0016-7037\(01\)00607-x](https://doi.org/10.1016/s0016-7037(01)00607-x).
- Tsui, M.T., Blum, J.D., Kwon, S.Y., 2020. Review of stable mercury isotopes in ecology and biogeochemistry. *Sci. Total Environ.* 716, 135386. <https://doi.org/10.1016/j.scitotenv.2019.135386>.
- U.S. EPA, 2002. Method 1631, Revision E: Mercury in Water by Oxidation, Purge and Trap, and CVAFS; U.S. EPA, Washington, D.C.
- U.S. EPA, 2024. Superfund Sites in Reuse in Utah. <https://www.epa.gov/superfund-redevelopment/superfund-sites-reuse-utah>.
- Utah Geological Survey, 2024. Energy and Minerals: Metals. <https://geology.utah.gov/energy-minerals/metals/>.
- Valdes, C., Black, F.J., Stringham, B., Collins, J.N., Goodman, J.R., Saxton, H.J., Mansfield, C.R., Schmidt, J.N., Yang, S., Johnson, W.P., 2017. Total mercury and methylmercury response in water, sediment, and biota to destratification of the Great Salt Lake, Utah, United States. *Environ Sci Technol* 51 (9), 4887–4896. <https://doi.org/10.1021/acs.est.6b005790>.
- Waddell, B., Cline, C., Darnall, N., Boeke, E., Sohn, R., 2009. Assessment of Contaminants in the Wetlands and Open Waters of the Great Salt Lake, Utah, 1996–2000. U.S. Fish and Wildlife Service.
- Weiss-Penzias, P.S., Gay, D.A., Brigham, M.E., Parsons, M.T., Gustin, M.S., Ter Schure, A., 2016. Trends in mercury wet deposition and mercury air concentrations across the U.S. and Canada. *Sci. Total Environ.* 568, 546–556. <https://doi.org/10.1016/j.scitotenv.2016.01.061>.
- Woerndle, G.E., Tsui, M.T., Sebestyen, S.D., Blum, J.D., Nie, X., Kolka, R.K., 2018. New insights on ecosystem mercury cycling revealed by stable isotopes of mercury in

- water flowing from a headwater peatland catchment. Environ. Sci. Technol. 52, 1854–1861. <https://doi.org/10.1021/acs.est.7b04449>.
- Wurtsbaugh, W.A., Leavitt, P.R., Moser, K.A., 2020. Effects of a century of mining and industrial production on metal contamination of a model saline ecosystem, Great Salt Lake, Utah. Environ Pollut 266 (Pt 1), 115072. <https://doi.org/10.1016/j.envpol.2020.115072>.
- Yang, S., Johnson, W.P., Black, F.J., Rowland, R., Rumsey, C., Piskadlo, A., 2019. Response of density stratification, aquatic chemistry, and methylmercury to engineered and hydrologic forcings in an endorheic lake (Great Salt Lake, U.S.A.). Limnol. Oceanogr. 65 (5), 915–926. <https://doi.org/10.1002/limo.11358>.
- Yin, R., Krabbenhoft, D.P., Bergquist, B.A., Zheng, W., Lepak, R.F., Hurley, J.P., 2016. Effects of mercury and thallium concentrations on high precision determination of mercury isotopic composition by Neptune Plus multiple collector inductively coupled plasma mass spectrometry. J. Anal. At. Spectrom 31 (10), 2060–2068. <https://doi.org/10.1039/c6ja00107f>.